# Rewiring the Three-Carbon Metabolism Abrogates Multiple MAPK-Induced Cellular Dysfunctions During Metabolic Disorder

Alexandre K. Dubé*[1], Nicolas Malenfant*[1], Florence Ladonne*[1], Amanda Piano[3], Karamat Mohammad[3], Marc Bélanger[1], Frédéric Bégin[2], Florence LeBel-Guay[1], Vladimir I. Titorenko[3] and Yves Bourbonnais[1,4]

[1]Département de biochimie, microbiologie et bio-informatique, [2]Département de biologie, Institut de biologie intégrative et des systèmes, Université Laval, Québec, Qc, Canada and [3]Department of Biology, Concordia University, Montreal, Qc, Canada

* These authors contributed equally to the study

[4]Correspondence: Yves Bourbonnais, Département de biochimie, microbiologie et bio-informatique, Pavillon C.-E.-Marchand, Université Laval, 1030 av. de la médecine, Québec, Qc, Canada G1V 0A6

E-mail: Yves.Bourbonnais@bcm.ulaval.ca

**SUMMARY**

Loss of membrane raft integrity, metabolic dysregulation and inflammation are hallmarks of chronic diseases and aging. It is not well understood how the stress response itself may contribute to the manifestation of these common traits. To explore this question, we screened the model organism *S. cerevisiae*, for the secretion of glycosylphosphatidylinositol-anchored proteins (GPI-APs) as a proxy for membrane raft instability. It is shown here that the multiple cellular dysfunctions previously described for a defect in the methylation pathway for phosphatidyl choline (PC) synthesis (*opi3Δ*) are linked with GPI-APs secretion. They collectively result from the sustained activation of the mitogen-activated protein kinase (MAPK) Hog1p. Through modifying the dihydroxyacetone phosphate / glycerol-3-phosphate ratio, activated MAPK promotes phospholipid gene de-repression and interferes with GPI anchor synthesis. Rewiring the three carbon metabolism, namely by deleting the mitochondrial glycerol phosphate dehydrogenase, abrogated the *opi3Δ* mutant pleiotropic phenotypes identifying key targets to counteract MAPK-induced cellular dysfunctions.

## INTRODUCTION

Aging is the greatest risk factor for many chronic diseases and, conversely, the establishment of a chronic illness may contribute to premature aging (Kennedy et al., 2014). Defective cellular processes and stress responses are shared between seemingly unrelated pathologies (*e.g.* type II diabetes (T2D), Alzheimer and Parkinson diseases) and aged cells. Among these, chronic endoplasmic reticulum (ER) stress, alteration in the composition of membrane microdomains rich in sphingolipid and cholesterol ("membrane raft" or "lipid raft") and inflammation often co-occurred in degenerative diseases (Boslem et al., 2013; Hummasti and Hotamisligil, 2010; Marin et al., 2016; Sprenkle et al., 2017; Tao et al., 2018) and during aging (Franceschi and Campisi, 2014; Martinez et al., 2017; Ohno-Iwashita et al., 2010). Furthermore, metabolic dysregulation is now recognized as an important modifier of numerous chronic diseases (Cai et al., 2012; Kennedy et al., 2014). The connection between various cellular processes defective in a plethora of conditions with the metabolism is, however, not well understood at the cellular level. In addition, it is unclear to what extent the stress response itself, when chronically activated, might contribute to metabolic dysregulation.

The yeast *S. cerevisiae* model organism has proved useful in providing mechanistic insights between altered basic cellular functions and neurodegeneration (Khurana and Lindquist, 2010; Tardiff et al., 2014) and nutrient sensing pathways involved in aging (Longo et al., 2012). An intimate connection between replicative aging, growth rate and the "environmental stress response" (ESR) was also recently described in yeast (Hendrickson et al., 2018). The aged-associated metabolic decline and chronic diseases of higher eukaryotes may therefore benefit from studies conducted in yeast aiming to understand the intricate connection between metabolic dysfunction and stress response.

Glycosylphosphatidylinositol (GPI)-anchored proteins (GPI-APs) are ubiquitous in eukaryotes and they localize primarily to membrane rafts (Brown and Rose, 1992; Fiedler et al., 1993). In yeast, GPI anchor synthesis is essential (Leidich et al., 1994) and disruption of most of the numerous genes involved in its synthesis causes lethality (Orlean, 2012). Many steps in the synthesis and remodeling of this glycolipid anchor involved substrates that are shared with other metabolic pathways. We therefore hypothesized that metabolic disorders, whether directly or indirectly, might affect completion and/or transfer of the GPI moiety to GPI-APs. Abortion at multiple steps of the GPI anchor synthesis or remodeling process leads to the secretion of anchor-less or incompletely matured GPI-APs, respectively (Li et al., 2006). We thus performed a genome-wide screen from the yeast knock-out (YKO) collection of non-essential genes to identify mutants hypersecreting two yeast model GPI-APs, Yps1p and Gas1p, as a proxy for alteration or loss of integrity in membrane rafts. In addition to test the hypothesis that mutations affecting the metabolism might be recovered by this approach, the objective of this study was to explore the mechanism by which stable association of GPI-APs to membrane rafts was compromised in one of these mutants.



Among the mutants identified, most of them unlinked to GPI anchor synthesis, the yeast *opi3Δ* mutant is the object of the present report. This mutant is defective in the last two methylation steps of the phosphatidylcholine (PC) biosynthesis pathway from phosphatidylethanolamine (PE) (McGraw and Henry, 1989). Mice deficient for the orthologous gene (PEMT) develop hepatic steatosis due to a reduced PC/PE when fed a normal diet (Li et al., 2006) whereas PEMT overexpression is associated with greater risks of obesity and T2D (Fu et al., 2011). However, in contrast to the mammalian PEMT enzyme that carries all methylation steps, in yeast the Cho2 enzyme is responsible for the first methylation step. Hypertrophied or supersized lipid droplets

(SLDs) was previously reported to develop in the *opi3Δ* yeast mutant when grown in synthetic complete (SC) medium and this was associated with an increase in phosphatidic acid (PA) (Fei et al., 2011). It was later demonstrated that the remarkable robustness of the *opi3Δ* mutant to lipid imbalance was due to an extensive reprograming of gene expression, referred to as the "membrane stress response" (MSR) (Thibault et al., 2012). More recently, a mitophagy defect resulting in part from the conjugation of Atg8p to monomethyl phosphatidylethanolamine (MMPE), that arises from conversion of PE by Cho2p, was described for the *opi3Δ* mutant (Henry et al., 2014; Sakakibara et al., 2015). This suggested sustained transcriptional upregulation of phospholipid (PL) biosynthetic genes in this mutant, which characterizes ER stress both in yeast (Travers et al., 2000) and animal cells (Hofbauer et al., 2014). In yeast, transcriptional regulation of PL biosynthetic genes is under the negative control of Opi1p (Henry et al., 2014). Opi1p repressor activity is modulated by its shuttling between the nucleus and ER membrane through binding with phosphatidic acid (PA) and the ER-membrane resident protein Scs2p (Loewen et al., 2004).



Using a combination of reverse genetics, biochemical and cell biology methods, lipidomic, and previously published proteomic data (Thibault et al., 2012), our study uncovered that sustained activation of the mitogen-activated protein kinase (MAPK) /Hog1p plays a key role in PL genes de-repression. In the *opi3Δ* mutant context, the Cho2-catalyzed conversion of PE into MMPE interferes with GPI anchor synthesis and is responsible for loss of membrane raft integrity. Rewiring the three-carbon metabolism in the *opi3Δ* mutant (*e.g.* disruption of either the *GPP2* or *GUT2* genes) potently suppresses these pleiotropic phenotypes. Globally, our study supports a model whereby activation of the MAPK/Hog1p signaling pathway exacerbates the phenotypes caused by lipid imbalance. This contributes to perpetuate its activation. Rewiring the central carbon metabolism around Gro-3-P to lower the DHAP/Gro-3-P ratio breaks down this vicious cycle.

Down regulation of p38 MAPK phosphorylation (Eriksson and Nystrom, 2014) and mGPD function (Madiraju et al., 2014), orthologs of the yeast Hog1p and Gut2p respectively, has been proposed for the mode of action of the anti-glycemic metformin, The intricate connection uncovered in the yeast model between the stress response and central metabolism might therefore be relevant to help understanding more complex pathologies in humans.

## RESULTS

### Loss of GPI proteins into the extracellular milieu is increased in mutants displaying ER stress, cell wall and/or vacuolar/lysosomal defects



The approach to identify yeast mutants that release GPI-APs into the medium with the two model proteins Gas1p and Yps1p is depicted Fig. 1. Media from 96-well yeast cultures grown for 48 h in synthetic complete medium were transferred onto nitrocellulose sheets and first assayed for Gas1p immunoreactivity (*Step 1*). Top ~10% Gas1p over-secretors (B-score above 2; 559 mutants, *see* Star Methods) were selected, cultured under the same conditions, and then assayed for extracellular Yps1p immunoreactivity. By arbitrary choosing a threshold corresponding to a 1.5-fold increase in the release of Yps1p compared to WT, 35 mutants were shown to release substantial amounts of both model GPI-APs into the medium (*Step* 2; *p*-values ranging from 3.45E-08 to 5.00E-02; $n = 3$; Table S1). Of these, 25 are either hypersensitive to the drugs *C*alco*f*luor *W*hite or *C*ongo *R*ed (CFW$^s$ and CR$^s$; Fig.1; Table S1), commonly used to detect cell wall deficiencies (Lussier et al., 1997), and 20 were previously shown to trigger the UPR response (Fig.1; Table S1)(Jonikas et al., 2009). As suggested by the reported sensitivity to Mefloquine (Sukhai et al., 2013), an antimalarial drug that disrupts vacuoles/lysosomes, several mutants (15/35) have some kind of vacuolar deficiency and, overall, 9 mutants display all three phenotypes (Fig. 1 *Step 2*; Table S1).

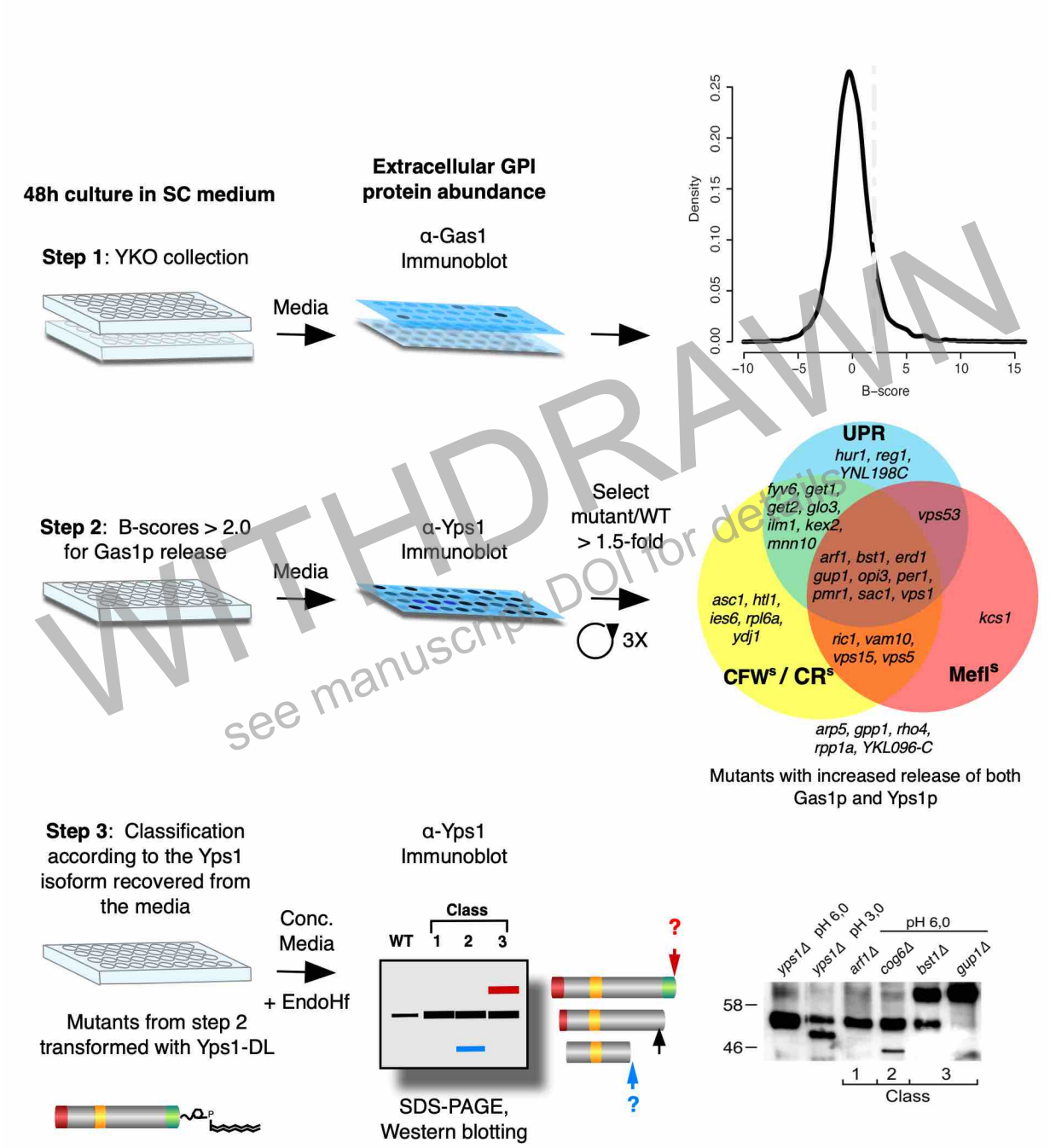




**Figure 1. Outline of the screening approach for identifying yeast non-essential mutants secreting GPI proteins in the extracellular *milieu***

The yeast mutant collection was screened for the secretion of GPI-APs, first for Gas1p (*Step 1*). Mutants with a B-score > 2.0 were further assayed for the secretion of Yps1p (*Step* 2) and then classified (*Step 3*) according to the major Yps1p molecular species recovered in the medium (*see* text and Table S1 for more details).

Using YeastMine (http://yeastmine.yeastgenome.org/yeastmine/bag.do; (Cherry et al., 2012); Table S1), the top 35 mutants were enriched for the biological process GO:0032507: maintenance of protein location in cell ($p$ = 9.52E-03) and the cellular components GO:0005794: Golgi apparatus ($p$ = 2.30E-6), GO:0000139 Golgi membrane ($p$ = 6.36E-5), GO:0012505: endomembrane system ($p$ = 1.74E-4) and GO:0098588 bounding membrane of organelle ($p$ = 3.2E-3). No enrichment was detected for the GO annotation: molecular function.

Yps1p is a two-subunit endopeptidase with alternate cleavage sites within a loop region, several soluble forms are thus associated with its release into the medium (Gagnon-Arsenault et al., 2008). To facilitate classification of the mutants according to the nature of the isoform released in the medium, an engineered single-chain Yps1p (Yps1-DL; (Dube et al., 2015)) expressed from a 2µ plasmid was transformed into each of the mutants (Fig. 1 *Step* 3). Concentrated proteins from the medium were then treated with Endo $H_f$ prior to SDS-PAGE, to reduce heterogeneity due to N-glycosylation, and Yps1 species were immunodetected with an anti-Yps1 antiserum. In WT yeast, self-shedding of Yps1-DLp at pH 6.0 occurs at an internal site, tentatively identified as $K^{498}$ (Dube et al., 2015) (Fig. 1 *Step 3*; *black arrow*), and the molecular weight (MW) of the major species secreted is ~ 53 kDa. Mutants predominantly secreting this species are referred to class 1 mutants (21/35). In class 2 mutants (7/35 mutants), an additional Yps1 isoform of (~46 kDa) was also present whereas in class 3 mutants (5/35), a high MW species (~66 kDa), alone (*gup1Δ, fyv6Δ and opi3Δ*) or with the characteristic ~53 kDa form (*bst1Δ* and *per1Δ*), was the predominant isoform observed. Secretion of high MW isoforms of GPI-APs in class 3 mutants were confirmed in untransformed strains for native Yps1 and Gas1p (Fig. S1). This suggested that in class 3 mutants, shedding of GPI-APs occurs near the GPI attachment site (Fig. 1 *Step 3*; *red arrow*).

**Class 3 mutants suggest an interplay between phospholipid imbalance, GPI anchor lipid synthesis and/or remodeling and the integrity of membrane microdomain**

Three of the five class 3 mutants are genes involved in GPI remodeling; *BST1* encodes an inositol deacylase (Fujita et al., 2006b; Tanaka et al., 2004); *PER1* is required for GPI-phospholipase A2 activity that remodels the GPI anchor (Fujita et al., 2006a) and; *GUP1*, a homolog of the Hedgehog pathway modulator HHATL (Hofmann, 2000), is required for addition of C26:0 fatty acid at the *sn*-2 position in GPI anchors (Bosson et al., 2006). The *OPI3* gene encodes a phospholipid methyltransferase involved in phosphatidylcholine (PC) biosynthesis (Fig. 2A) (Kodaki and Yamashita, 1987) whereas the *FYV6* gene is poorly characterized. Mutants with defects in either GPI anchor lipid remodeling (*per1Δ*), phospholipid synthesis (*opi3Δ*) or loss of Fyv6p (*fyv6Δ*) were previously shown to promote the disappearance of marker proteins from an ergosterol-rich membrane raft compartment known as the MCC compartment (*M*embrane *C*ompartment of *C*an1) (Grossmann et al., 2008). Hence, loss of GPI-APs in the medium correlates with membrane raft alterations and/or dynamics in these mutants. The finding that *opi3Δ* yeast releases GPI-AP isoforms similar to that observed for GPI lipid remodeling mutants also suggested that defects in phospholipid synthesis influences GPI biosynthesis, anchoring and/or remodeling.

Defects in GPI anchor acyl chain remodeling (*bst1Δ*, *per1Δ* and *gupΔ*) (Bosson et al., 2006; Castillon et al., 2009; Fujita et al., 2006a) and in *opi3Δ* (Thibault et al., 2012) were previously reported to delay exit of GPI-APs from the ER. As shown by western blotting, we confirmed that in the *opi3Δ* mutant ER forms of both Gas1p (~105 kDa; (Fankhauser and Conzelmann, 1991)) and Yps1p (~85 and ~100 kDa; (Kajiwara et al., 2008)) accumulated within the cells (Fig. 2B). In contrast, very little of the mature hyperglycosylated Yps1p, running as a smear between the 135-

and 190-kDa markers, or Gas1p (~125 kDa) were cell-associated and most of these mature species were recovered in the medium.

In *opi3Δ* yeast, synthesis of PC from the methylation pathway using CDP-DAG is blocked (Fig. 2A) (McGraw and Henry, 1989). PC levels in this mutant are maintained through the alternative Kennedy pathway that uses DAG and CDP-choline (Kennedy and Weiss, 1956), provided that choline is available from the growth medium. Several mutants involved in PC biosynthesis, including *opi3Δ*, were recently shown to produce SLD in SC medium but not on rich medium (YPD) (Fei et al., 2011). This phenotype was reversed by the addition of choline, indicating that this is linked to a reduced PC level, but also by the addition of inositol, whereas the addition of ethanolamine (EtN) did not correct this phenotype. To investigate whether the loss of GPI-APs in the medium also correlated with PC depletion when *opi3Δ* yeast was grown in synthetic medium, we compared the fraction of Yps1p recovered in the medium upon addition of each of these PL precursors. To facilitate quantification of the mature hyperglysosylated forms of Yps1p (smear centered at ~165 kDa; Fig. 2B) cell extracts and supernatants were treated with EndoH$_f$ (reducing both its heterogeneity and size to ~66 kDa; Fig. 2C). In the presence of a functional Opi3 enzyme, the release of Yps1p was negligible (~ 1% compared to ~60% in *opi3Δ* yeast) in any conditions, except with the addition of 1 mM choline that slightly stimulated its release (4% compared to 1%; Fig. 2C). However, this did not reach statistical significance ($p$ = 0.0663). More pronounced qualitative and quantitative changes were noted upon addition of PL precursors to the *opi3Δ* mutant. Unlike WT yeast, *opi3Δ* yeast cultured in the absence of PL precursors, or in the presence of choline, was largely missing the cell-associated Yps1p isoform (~66 kDa after EndoH$_f$ treatment; Fig. 2C). A species of similar size accumulated in the extracellular *milieu* of *opi3Δ* yeast,

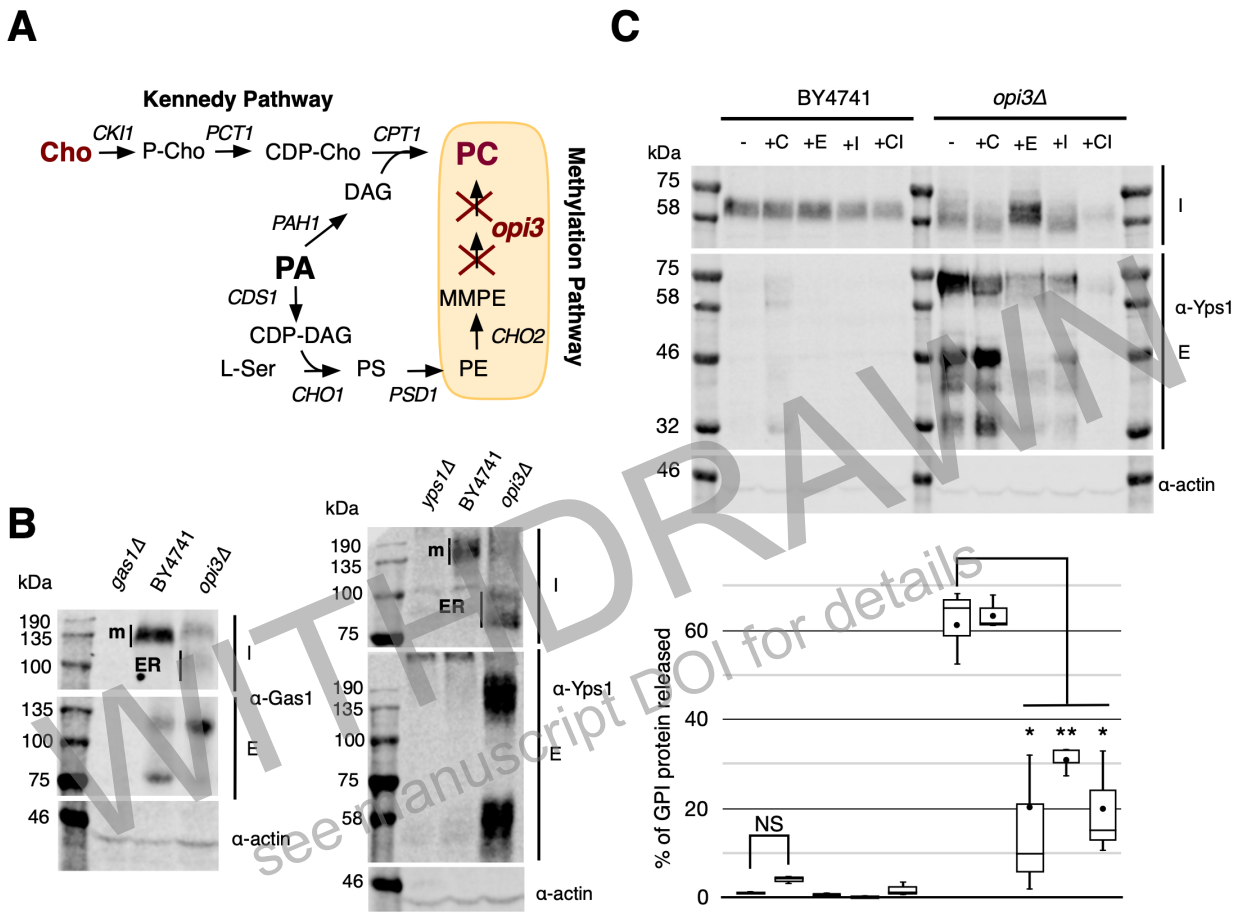


**Figure 2. Supplementation of lipid precursors, except choline alone, partially alleviates the loss of GPI-APs in the medium of the *opi3Δ* mutant.**

(A) Phosphatidylcholine (PC) biosynthesis by the Kennedy and the methylation pathways in which phosphatidic acid (PA) is a shared biosynthetic precursor.

(B) Western blotting of Gas1p (*left panel*) and Yps1p (*right panel*) from cell extracts (I) and media (E) of BY4741 and the *opi3Δ* mutant. In the absence of EndoHf treatment, the *opi3Δ* mutant accumulates the ER forms (ER) of both Yps1p and Gas1p while the bulk of the mature/hyperglycosylated form (m) is lost in the medium. Actin (α-actin) was used as a loading control and the *gas1Δ* and *yps1Δ* mutants as negative controls for the immunodetection with the Gas1 (α-Gas1) and Yps1 (α-Yps1) antisera, respectively.

(C) (*Top panel*) Representative western blot of Yps1p ($n$ = 3 biological replicates) from EndoH$_f$-treated cell extracts (I) and media (E) of the BY4741 and *opi3Δ* strains grown in the presence or absence of lipid precursors. Actin (α-actin) was used as a loading control. (*Bottom panel*) Box plot showing the mean percentage of Yps1p released in the medium (*filled circles*) with the first and third quartiles, the median, and the maximum and minimum values. NA: No addition; +C: Choline 1 mM ; +E: Ethanolamine 1 mM ; +I: Inositol 75 µM ; +CI: Choline 1mM and inositol 75 µM. NS; not significant, *; $p < 0.05$, **; $p < 0.01$.

along with shorter species. The combined addition of choline and inositol (+CI; Fig. 2C), and intriguingly EtN (+E; Fig. 2C), stabilized cell association of the ~66 kDa species. However, the addition of EtN to *opi3Δ* yeast led to slow growth in SC medium and to achieve similar cell density, cultures were extended to 42 h compared to 20 h for all other samples. Consistently, none of the PL precursors restored to WT levels the relative amounts of GPI-APs released by *opi3Δ* yeast. Nonetheless, major decreases (>3-fold) were observed with all PL precursors, except with choline alone. Overall, this suggested that PC depletion and the pathway used to synthesize this glycerophospholipid (methylation vs Kennedy; Fig. 2A) influence the stability of GPI-APs. Given the critical role of EtN in GPI synthesis and anchor attachment (Kinoshita and Fujita, 2016), these data also suggested that the rapid conversion of PE to mono-methyl phosphatidylethanolamine (MMPE) by Cho2p (Thibault et al., 2012) restricts its availability for other metabolic pathways in the context of the *opi3Δ* mutant.



**Constitutive de-repression of *INO1* in the *opi3Δ* mutant in inositol limiting conditions is independent from the Snf1/AMPK kinase activity**

The *opi3-3* point mutant was initially identified as an *o*ver*p*roducer of *i*nositol (Opi- phenotype) (Greenberg et al., 1982). Ino1p, the rate-limiting enzyme in conversion of glucose-6-phospate (G-6-P) into *myo*-inositol, is constitutively expressed in *opi3Δ* mutants and can only be repressed by the addition of both inositol and choline (McGraw and Henry, 1989). PA plays a role in controlling de-repression of the *INO1* gene by modulating the shuttling of the Opi1 repressor between the nucleus and the ER membrane (Loewen et al., 2004). Upon inositol depletion, this results from the sequestration of Opi1p at the ER membrane through interaction with both Scs2p and PA (Fig. 3A). The strength of this binding was shown to be negatively correlated with the acyl chain length of PA (Hofbauer et al., 2014). De-repression of *INO1* in *opi3Δ* yeast growing in SC medium is

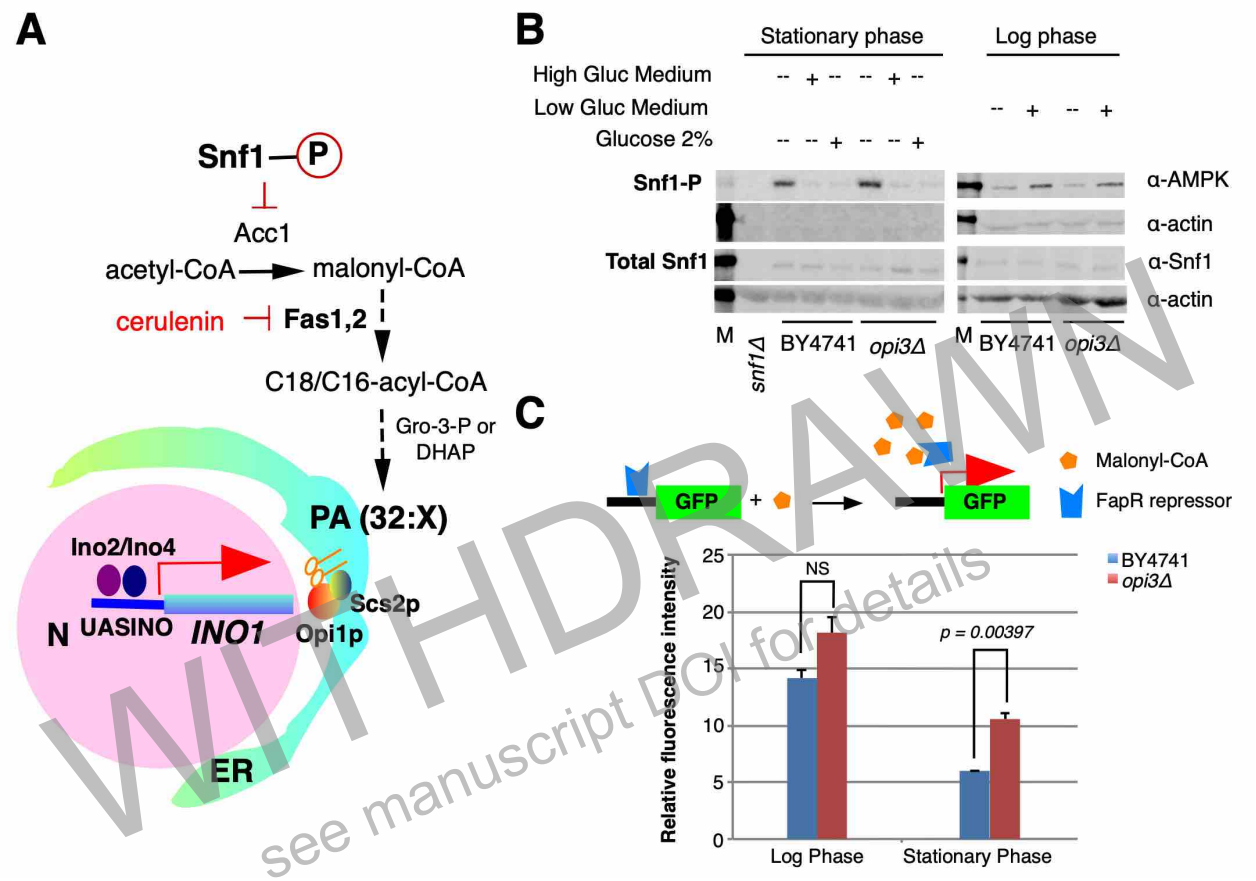




**Figure 3. Snf1/AMPK or Acc1 activities do not account for the increased accumulation of phosphatidic acid with short acyl chains in *opi3Δ* yeast growing in SC medium**

(A) Model of *INO1* gene de-repression based on Hofbauer et al., 2014.

(B) Representative western blots from stationary (*n=2*; *left panel*) and log phase (*n=3*; *right panel*) cultures of the indicated yeast strains grown in SC medium and shifted, or not, to high and low glucose SC medium or supplemented by 2% glucose for 30 min prior to total protein extraction. Phosphorylation of Snf1p was detected with a rabbit α-AMPK and total Snf1p with a goat α-Snf1, actin was the loading control (α-actin).

(C) Relative fluorescence intensity, in the presence of cerulenin, of the indicated yeast strains expressing the malonyl-CoA biosensor pFDA09 (David et al., 2016) grown to the indicated growth phase in SC medium. Data shown are mean +/- SD (*n=3*).

markedly more pronounced than that observed in WT yeast during the log phase (Thibault et al., 2012). As previously reported (Fei et al., 2011), and confirmed here by lipidomic analysis (Table S2), this correlates with an increased PA level in the *opi3Δ* mutant compared to that estimated in WT yeast (~ 2-fold; $p = 6.85E-04$). Furthermore, the relative proportion of short mono-unsaturated

acyl chain PA [32:1] was increased by ~ 24%, concomitantly with a ~ 29 % decrease in PA [34:1], in the *opi3Δ* mutant compared to WT yeast ($p$ = 0.0021 and 0.0008, respectively; Table S2).

Acetyl-CoA carboxylase (Acc1p), which catalyzes the conversion of Acetyl-CoA into malonyl-CoA, is known to regulate acyl chain length composition of phospholipids. Lowering its activity promotes *INO1* de-repression (Shirra et al., 2001). The Snf1 kinase, an ortholog of the mammalian AMP kinase, phosphorylates $Ser^{1157}$ of Acc1p to down-regulate its activity. This decreases the amount of malonyl-CoA and was shown to lower the PA C18/C16 acyl chain ratio ((Hofbauer et al., 2014); Fig. 3A). We thus hypothesized that the accumulation of PA with short acyl chains in *opi3Δ* might result from improper activation of Snf1 during the log phase growth in high glucose. However, phosphorylated Snf1-HA species from stationary phase cultures disappeared, both for WT and *opi3Δ* yeast, within 30 min after addition of either fresh glucose-containing SC medium or glucose alone (Fig. 3B; *left panel*). The reciprocal experiment also indicated that Snf1-HA becomes similarly phosphorylated in both strains upon switching log phase cultures to low glucose medium for 30 min (Fig. 3B; *right panel*).

Using a malonyl-CoA sensor as a proxy for Acc1 activity (David et al., 2016), we also found that in the presence of cerulenin, an inhibitor of the fatty acid synthase complex (Fig. 3A), log or stationary phase cultures of *opi3Δ* yeast accumulate higher amounts of malonyl-CoA compared to WT yeast (Fig. 3C). Globally, these data therefore do not support that a reduced Acc1p activity in *opi3Δ*, compared to that of WT, is responsible for the greater *INO1* de-repression in the mutant strain.

**Activation of the Hog1/MAPK signaling pathway is part of the *opi3Δ* membrane stress response**

Acylation of Gro-3-P is the common and universal route to form PA, but the glycolytic intermediate

DHAP can also be used (Athenstaedt et al., 1999). Prior studies in yeast demonstrated that *SCT1/GAT2* encodes a Gro-3-P acyl transferase (GAT) with a net preference for C16 acyl-CoA but poorly acylates DHAP. In contrast, the GAT encoded by *GPT2/GAT1* similarly acylates DHAP and Gro-3-P with no preference for C16 over C18 acyl-CoA (Zheng and Zou, 2001). We thus considered the possibility that a shift toward DHAP for lyso-PA synthesis might enrich for C16-containing species catalyzed by Sct1p in the pool of lyso-PA derived from Gro-3-P. This would result from a decrease availability of Gpt2 for acylation of Gro-3-P (Fig. 4A). In this scenario, the higher the DHAP/Gro-3-P ratio available for lyso-PA synthesis, the higher the enrichment for short acyl chain PA species derived from Gro-3-P. As a consequence, however, this latter pool of PA would be smaller than the one derived from DHAP (Fig. 4A). What cellular mechanism could operate this shift?



The log phase proteome of *opi3Δ* is broadly modified relative to WT yeast (Thibault et al., 2012). Increased levels of the mGPD and 1-acyl DHAP reductase, encoded respectively by the *GUT2* and *AYR1* yeast genes, were previously observed in log phase cells of the *opi3Δ* mutant ((Thibault et al., 2012); Fig. 4C). Genes up- and down-regulated in response to a hyperosmotic shock (Rep et al., 2000) also overlap with the relative abundance of the corresponding proteins in *opi3Δ* compared to WT yeast (Fig. S2). This suggests that growth in the absence of inositol, at least for the *opi3Δ* mutant, activates the MAPK/Hog1 signaling pathway. Combined with the Gut2-catalyzed re-oxidation of Gro-3-P into DHAP and the Hog1-P-stimulated glycerol production from Gro-3-P, this would promote a higher DHAP/Gro-3-P ratio. The ratio of dually phosphorylated Hog1-GFP (Hog1-P-GFP; α-p38) over total Hog1-GFP (α-GFP) was confirmed to be greater in the *opi3Δ* mutant grown in the absence of lipid precursor compared to that of WT yeast cultured under any condition (Fig. 4B; *p values* of 0.0463, 0.0209 and 0.0209 *vs* BY4741, BY4741 + I and BY4741 +

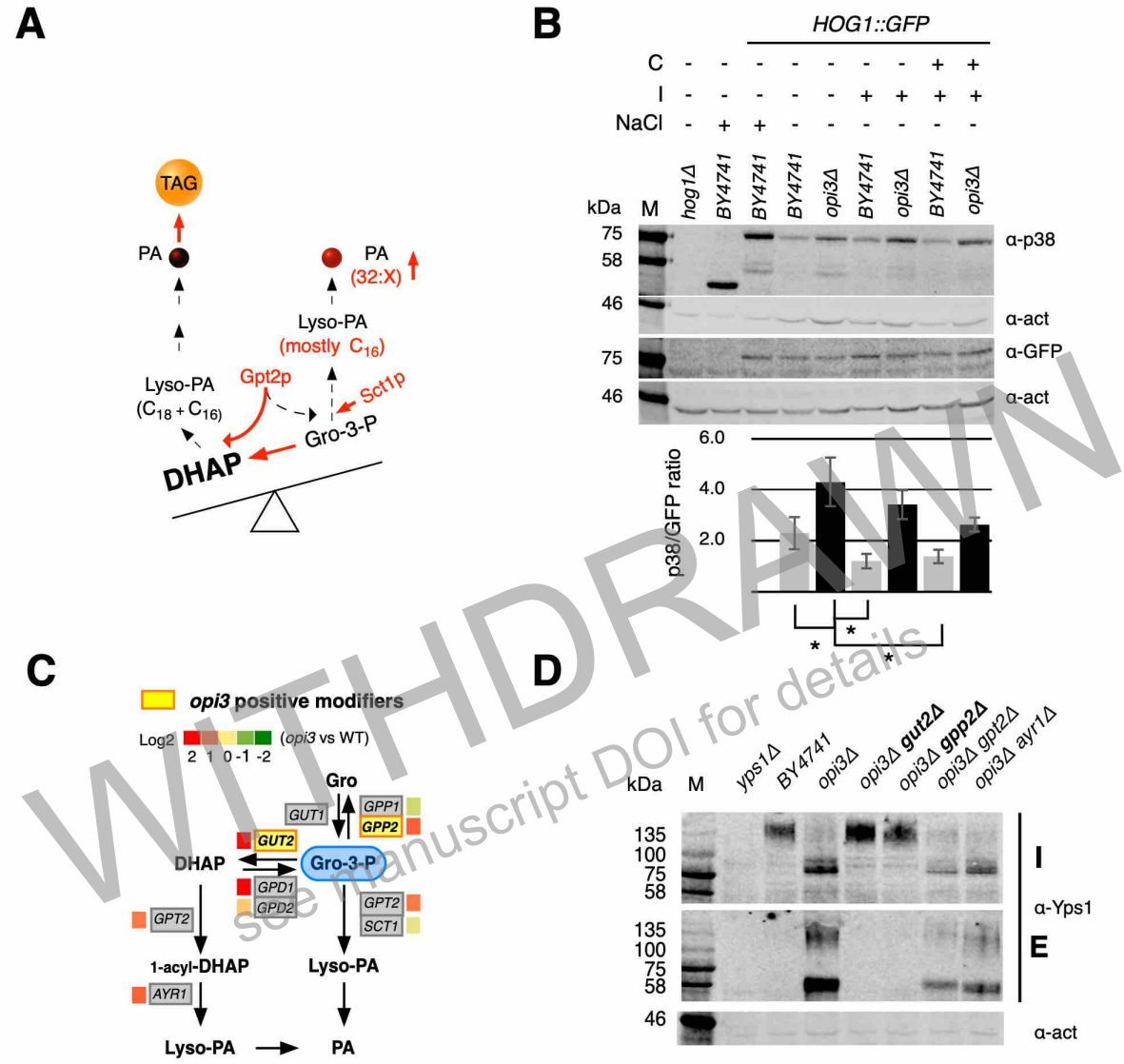




**Figure 4. Basal MAPK/ Hog1p phosphorylation is increased in *opi3Δ* yeast and deletion of key effectors rescues GPI-AP stability at the cell surface**

(A) Scheme illustrating how a shift toward DHAP can favor the formation of a small (Gro-3-P-derived) pool of PA enriched for short acyl chains (32:X).

(B) Representative western blot ($n$ = 3) of total protein extract from the indicated strains carrying or not *HOG1::GFP* grown to early log phase in SC medium and supplemented, or not, with 75 µM inositol (I) and 1 mM choline. Dually phosphorylated Hog1 or Hog1-GFP was detected with a rabbit antiserum against p38 (α-p38) and Hog1-GFP with a rabbit antiserum against GFP (α-GFP). Positive control for Hog1 phosphorylation was BY4741 or *HOG1::GFP* cultures incubated 5 min with 0.5 M NaCl. Negative control for the immunodetection was the *hog1Δ* strain. Actin was the loading control (α-act). The bar graph shows the Hog1-P/Hog1-GFP ratio +/- SD. *; $p < 0.05$.

(C) Genes implicated in Gro-3-P utilization were each deleted in the *opi3Δ* background and positive modifiers are highlighted (*yellow boxes*). The heatmap represents the relative abundance of the enzymes found in the *opi3Δ* mutant over WT yeast from the proteomic data of Thibault et al., 2012.

(D) Representative western blot ($n$ = 3) showing the intracellular (I) and extracellular (E) distribution of Yps1p in the single and double *opi3Δ* mutants. Actin was the loading control (α-act).

CI, respectively). This therefore supports the view that in inositol-limiting conditions de-repression of *INO1* in *opi3Δ* yeast implicates the following mechanism; a shift toward DHAP-derived PA and a relative enrichment of another pool of PA with short acyl chains through activation of the MAPK/Hog1 signaling pathway.

If a shift toward an increase DHAP/Gro-3-P ratio is a determinant factor to promote *INO1* expression, modifying the flux around Gro-3-P might enable the identification of positive gene modifiers. This was tested by systematically deleting genes around Gro-3-P in the *opi3Δ* background (Fig. 4C). As a rapid assay we first monitored, through dot blot analysis, the release of the model GPI-AP Yps1 in the double mutants and two extragenic suppressors were identified; *gut2Δ* and *gpp2Δ* (Table S3). Western blotting with an anti-Yps1 confirmed that deletion of *GUT2* or *GPP2* in the *opi3Δ* yeast nearly completely prevents the release of Yps1p in the extracellular *milieu* (Fig. 4D). These modifiers additionally corrected, albeit to variable extent, the inositol secretion phenotype of the *opi3Δ* mutant (Opi- phenotype) and its slow growth (Fig. S3), as well as the accumulation of SLD as estimated by BODIPY 493/503 and Nile red staining (Fig. S4A&B). Furthermore, while the overall triacylglycerol (TAG) content was slightly lowered in the *opi3Δ gut2Δ* mutant, this was not statistically significant. In contrast, the TAG content was sharply and significantly reduced in *opi3Δ gpp2Δ* yeast (50%; *p*value = 0.02137) compared to the single *opi3Δ* mutant (Table S2).



**Positive modifiers of the *opi3Δ* mutant modify the phosphatidic acid species profile and down-regulate phospholipid gene transcription during growth in inositol limiting conditions**

According to the working model (Fig. 4A), the increased abundance of the PA 32:1 species in the *opi3Δ* would be mostly derived from acylation of Gro-3-P by Sct1p, because of an increased DHAP/Gro-3-P ratio. Deletion of either the *GUT2* or *GPP2* gene, by respectively preventing re-

oxydation of Gro-3-P into DHAP or its conversion into glycerol, would thus be expected to decrease this ratio and, consequently, to reduce the accumulation of the PA 32:1 species in the *opi3Δ* mutant. Lipidomic analysis confirmed this prediction as a significant decrease in PA 32:1 was detected in the *opi3Δ gut2Δ* (- 35%) and the *opi3Δ gpp2Δ* (- 18%) double mutants (Fig. 5A; Table S2). In both cases, this was accompanied by a substantial increase in PA 34:2 content.

The Opi1 repressor shuttles between the nucleus and ER membrane to de-repress PL gene synthesis and was reported to bind preferentially to PA with short acyl chains. In inositol depleted conditions, GFP-tagged Opi1 was found predominantly around the perinuclear region, composed of the nuclear and ER (nER) membranes (Gaspar et al., 2017; Hofbauer et al., 2014; Loewen et al., 2004; Romanauska and Kohler, 2018). In addition,, florescent dots at the cell periphery, possibly corresponding to the cortical ER (cER) making contact sites with the plasma membrane, were observed under these conditions (Gaspar et al., 2017; Hofbauer et al., 2014). Fluorescent punctate structures, suggested to be sites of nascent LD formation, were also recently reported in WT yeast expressing a similar Opi1-GFP reporter lacking its Scs2 binding domain (FFAT) and for full-length Opi1-GFP expressed in an *scs2Δ* mutant (Gaspar et al., 2017). The distribution of the reporter GFP-Opi1 in WT, *opi3Δ* and *opi3Δ gut2Δ* cells in relationship with their PA molecular species distribution was next analyzed (Fig. 5B).

From the transformants displaying fluorescence, the characteristic staining of GFP-Opi1 at the perinuclear ER (nER) membrane was observed in 64% of WT yeast, 71% of the *opi3Δ* mutant and 60% of the *opi3Δ gut2Δ* double mutant when cultured to the mid-log phase in inositol limiting conditions. However, nER staining of GFP-Opi1 was noticeably weaker in the the *opi3Δ* mutant compared to WT yeast. In contrast, fluorescence associated to "puncta" was more frequently observed in the *opi3Δ* mutant (48%) than in WT cells (20%). The closed vicinity of fluorescent

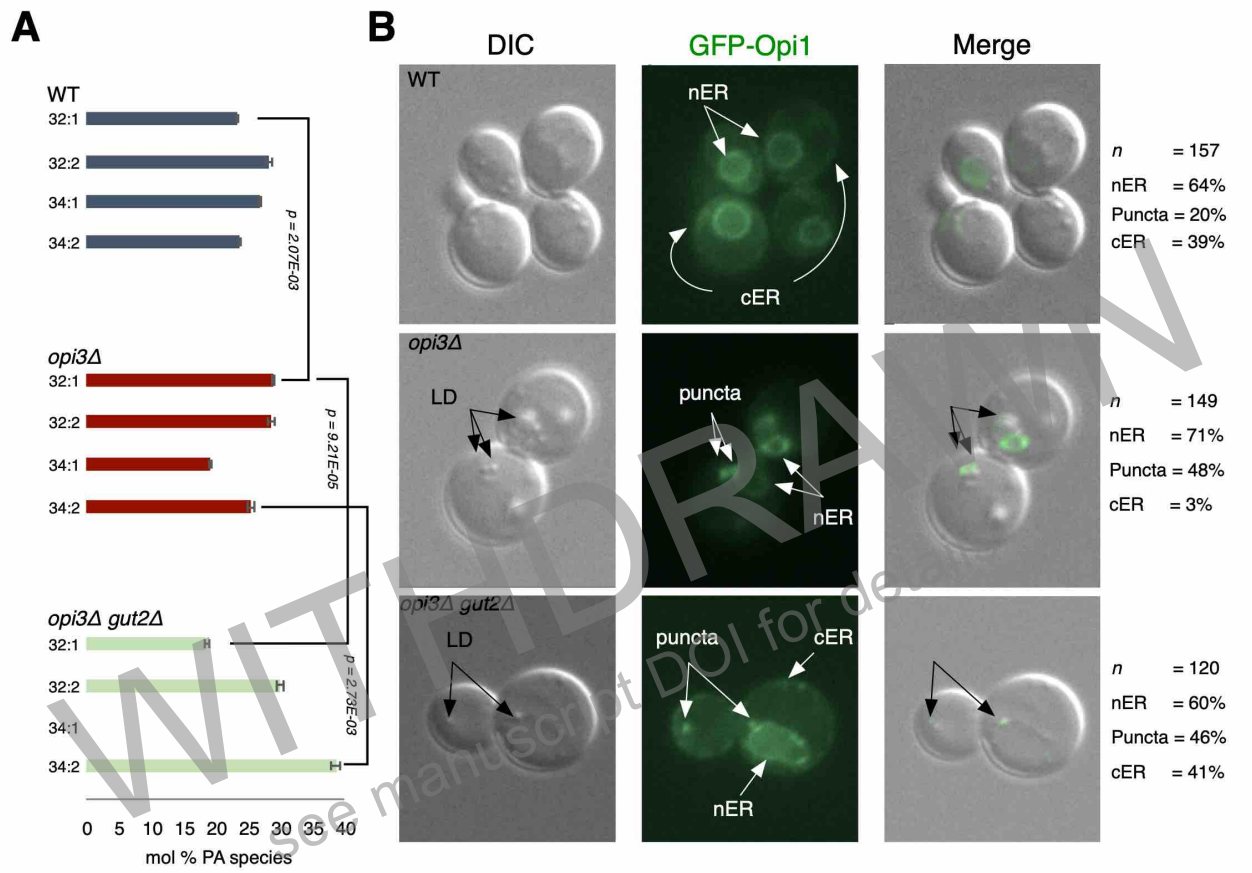


**Figure 5. Correction of the *opi3Δ* defects is associated with changes in phosphatidic acid composition and GFP-Opi1p localization**

(A) Mole percentage (Mol %) content +/- SD ($n$ = 3) of each phosphatidic acid (PA) species detected by lipidomic analysis from the WT, *opi3Δ* and *opi3Δ gut2Δ* yeast strains.

(B) Relative distribution (*right*) and representative micrographs of the GFP-Opi1 localization in the indicated transformed yeast strains grown to early log phase in SC medium. DIC; differential interference contrast, nER; perinuclear ER, cER; cortical ER, LD; lipid droplets.

punctate structures with LD, as observed in differential interference contrast (Fig. 5B) as well as by co-localization between the LD marker Erg6-mCherry and GFP-Opi1 (Fig. S5), supported the notion that these structures are sites of LD formation. Although a trend toward larger punctate structures was apparent for the *opi3Δ* mutant compared to WT yeast or the *opi3Δ gut2Δ* double mutant, the percentage of fluorescent *opi3Δ gut2Δ* cells with puncta was similar to that observed in the single *opi3Δ* mutant (46% vs 48%). Compared to WT (39%) or the *opi3Δ gut2Δ* double mutant (41%), few *opi3Δ* cells (3%) appear to display fluorescent dots at the cell periphery. As

these dots may have escaped visual inspection, due possibly to an overall lower intensity of GFP-Opi1 binding to the ER membrane (nER + cER, excluding the punctate structures), the cell periphery/perinuclear fluorescence pixel intensity ratios was also measured by freehand selection using Image Studio Lite (Fig. S6A). With a mean of 1.66 +/- 0.0.90 for the single *opi3Δ* mutant (*n* = 26 cells), this ratio was lower than that estimated for the WT (2.52 +/- 1.06; *p* = 7.2E-03) and the *opi3Δ gut2Δ* (4.70 +/- 2.33; *p* = 1.6E-06) mutant ratios. In line with the recent finding that the acute response to PC imbalance in the yeast *cho2Δ* mutant causes cER disappearance (Vevea et al., 2015), this suggests that the lower fluorescence intensity of GFP-Opi1p at the cell periphery in the *opi3Δ* mutant may partly be due to cER disappearance. Although other interpretations cannot be excluded, the deletion of *GUT2* restored the presence of GFP-Opi1p at the cell periphery suggesting re-appearance of the cER in the double mutant.



As estimated by qRT-PCR, deleting the *GUT2* gene in the *opi3Δ* mutant also substantially reduced *INO1* gene expression in SC medium (Fig. S6B). With a pvalue of 0.0525 however, transcriptional down-regulation of *INO1* possibly constitutes only one facet in the correction of the *opi3Δ* mutant pleiotropic phenotypes by the deletion of *GUT2*. Globally, these data support the view that the observed decrease in PA 32:1 in the *opi3Δ gut2Δ* double mutant results from lowering the DHAP/Gro-3-P ratio. This rewiring in the three-carbon metabolism is sufficient to restore GFP-Opi1p staining at the cell periphery while not completely eliminating Opi1p-bound punctate structures.

**Loss of GPI-APs in the *opi3Δ* mutant results from competition between the PC methylation and the GPI anchor biosynthetic pathways**

GPI anchor synthesis requires the addition of ethanolamine phosphate (EtN-P) on three mannose residues of the structure (Fig. 6A). These additions are catalyzed by the Mcd4, Gpi13 and Las21

phosphoethanolamine transferases, the first two enzymes being encoded by essential genes. *MCD4* is an essential gene because addition of EtN-P to the first mannose residue of the anchor is required to add the third mannose residue (Imhof et al., 2004). The EtN-P added to this third mannose residue by Gpi13 is then used to attach the GPI anchor to the protein (Flury et al., 2000; Taron et al., 2000; Toh-e and Oguchi, 2002). Our finding that ethanolamine (EtN) supplementation partially rescued the loss of mature Yps1 species from the *opi3Δ* cell surface (Fig. 2D) suggested that the relative abundance of PE (direct lipid precursor of EtN-P) in this mutant is very low, which impedes GPI anchor synthesis (Mcd4 and Gpi13). Given the massive accumulation of MMPE in the *opi3Δ* mutant (Thibault et al., 2012), and as the same pool of PE is used by the Cho2 and Mcd4 enzymes (Wilson-Zbinden et al., 2015), this could explain the loss of GPI-APs in the *opi3Δ* mutant.



To further document this, we compared the release of Yps1p between *cho2Δ*, *opi3Δ* and conditional temperature sensitive (ts) mutations in the essential genes *MCD4* and *GPI13* (*mcd4-174*, *gpi13-3* and *gpi13-5*, respectively), with or without a functional *CHO2* gene (Fig. 6B). As anticipated, despite sharing many phenotypes with *opi3Δ* (SLD, elevated PA levels, low PC levels and excretion of inositol; (Fei et al., 2011; Summers et al., 1988)) *cho2Δ* yeast did not release GPI-AP in the medium. In contrast, the conditional ts mutants secreted either small (*mcd4-174* and *gpi13-3*) or large (*gpi13-5*) amounts of Yps1p in the medium relative to *opi3Δ* yeast, even at the permissive temperature (30 $^{0}$C). They also accumulated the ER forms of Yps1p (asterisks in Fig. 6B). Deleting *CHO2* in the *gpi13-5* ts mutant nearly completely abrogated the loss of Yps1p in the medium and the accumulation of the ER forms.

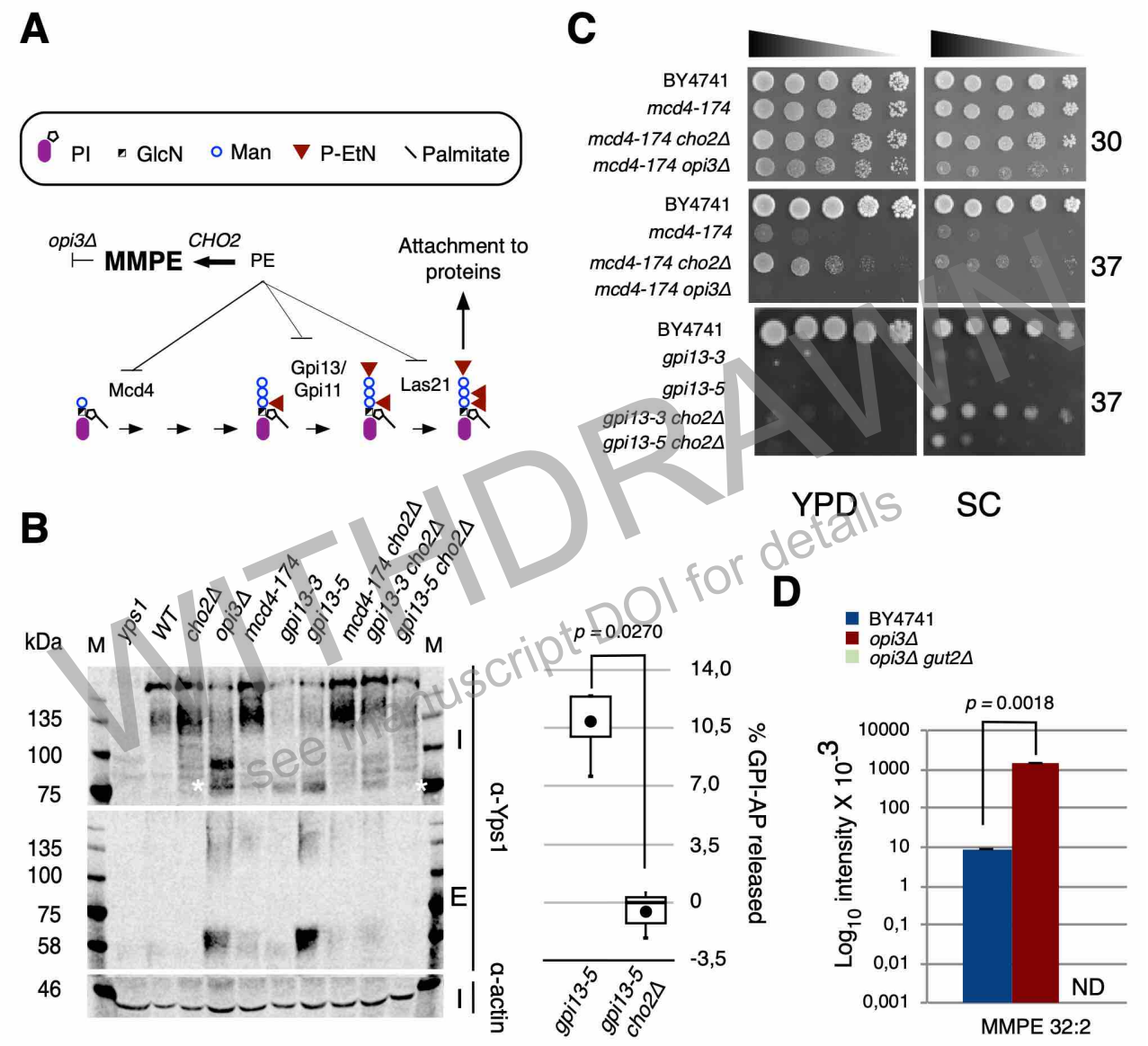




**Figure 6. Secretion of GPI proteins in the *opi3Δ* mutant results from deficiency in GPI anchor attachment**

(A) Cartoon illustrating the competition for the shared substrate PE between Cho2p and the three phospoethanolamine transferases involved in GPI biosynthesis (Mcd4p, Gpi13p and Las21p).

(B) Representative western blot ($n$ = 3; *left panel*) showing the intracellular (I) and extracellular (E) distribution of Yps1p in GPI biosynthetic versus phospholipid mutants. Actin was used as a loading control. Asterisks point to the ER form of Yps1p. Box plot (*right panel*) derived from the western blots illustrating the significant difference between the release of Yps1p from the *gpi13-5* and *gpi13-5 cho2Δ* yeast mutants.

(C) Spotting assays illustrating the genetic interactions between *CHO2*, *OPI3*, *MCD4* and *GPI13* on rich (YPD) and synthetic medium (SC) at $30^0$C and/or $37^0$C.

(D) Relative abundance of MMPE 32:2 as measured by lipidomic analysis.

If competition for PE is determinant for the release of GPI-APs by *opi3Δ* yeast, deleting *OPI3* in *mcd4-174*ts or *gpi13*ts should exacerbate the growth defect. This was confirmed as the growth of the *opi3Δ mcd4-174*ts double mutant on YPD and SC plates was further affected, at 30ºC or 37ºC (Fig. 6C). Furthermore, all attempts to construct double mutants harboring an *opi3Δ* null allele in the *gpi13*ts background failed. Conversely, deleting the *CHO2* gene in any of these ts mutants enabled their growth at the restrictive temperature (Fig. 6C). Accumulation of MMPE in *opi3Δ* is indicative of this competition between Cho2p and the PE transferases Mcd4, Gpi13 and Las21 (Fig. 6A). As all positive modifiers of *opi3Δ* restored membrane-bound mature GPI-Yps1p (Fig. 4D), this suggested that Cho2p no longer competes for PE in the *opi3Δ gut2Δ* and *opi3Δ gpp2Δ* double mutants. Lipidomic analysis confirmed this prediction. The relative intensity of MMPE species was two orders of magnitude higher in *opi3Δ* than WT yeast and no peaks ascribed to MMPE could be detected in the *opi3Δ gut2Δ* and *opi3Δ gpp2Δ* double mutants (Fig. 6D; Fig. S7).



The accumulation of MMPE in the *opi3Δ* mutant was recently shown to be linked with a mitophagy defect due, in part, to the conjugation of MMPE to Atg8 (a PE-conjugated ubiquitin-like modifier involved in all autophagy-related processes) (Sakakibara et al., 2015). The autophagic flux, estimated by vacuolar hydrolysis of GFP-Atg8 to free GFP, was markedly impaired. We found that the *opi3Δ* modifiers (*opi3Δ gut2* and *opi3Δ gpp2* double mutants) also corrected this abnormal autophagic flux and in fact, stimulated the formation of free GFP to levels exceeding that observed in WT yeast in addition to lowering the overall relative amount of total Atg8p (Fig. S8A). Furthermore, unlike the *cho2Δ* mutant used as a control and the *opi3Δ gut2* and *opi3Δ gpp2* double mutants, the *opi3Δ* single mutant was exquisitely sensitive to the autophagic inducer rapamycin at 5 ng/mL (Fig. S8B). In sum, most observable defects of the *opi3Δ* mutant could be corrected by the deletion of either Gut2p or the MAPK/Hog1-induced effectors Gpp2p.

## DISCUSSION

The aim of this study was to investigate which and how perturbed cellular functions promote the release and/or shedding of GPI proteins in the extracellular milieu using the yeast *S. cerevisiae* as an experimental model. A previous screen performed with the yeast GPI cell wall-associated protein α-agglutinin (GFP-Sag1p; (Gonzalez et al., 2010)), and restricted to strains deleted for genes involved in cell wall biogenesis (167 diploid strains), identified eight hypersecretors. Heterozygotes for the essential genes *MCD4* and *GPI13* were among these. As reported here, screening the non-essential yeast knock-out collection for the loss of model GPI proteins (Gas1p and Yps1p) in the medium uncovered several additional genes, most showing hypersensitivity to cell wall perturbing agents (23/30 mutants: Fig. 1). A detailed characterization of the *opi3Δ* mutant highlighted a metabolic link between deficiencies in glycerophospholipid biosynthesis and the essential genes *MCD4* and *GPI13* involved in GPI anchor synthesis. Specifically, in the absence of both choline and inositol, de-repression of phospholipid biosynthetic genes in the context of the *opi3Δ* null mutation drives the conversion of PE to MMPE by Cho2p. The resulting shortage in PE compromises EtN-P transfer to the GPI anchor hence precluding its completeness and/or its attachment to GPI-APs. As initially suggested by the increased amount of membrane-bound mature GPI-Yps1p upon supplementation of *opi3Δ* with EtN, this conclusion is supported by the fact that the *cho2Δ* mutant do not secrete GPI-APs and by the finding that MMPE was sharply reduced in the *opi3Δ* positive modifiers. Furthermore, in line with the previously reported observation that autophagy, GPI anchor synthesis and the PC methylation pathway share the same pool of PE (Wilson-Zbinden et al., 2015), positive modifiers also corrected the autophagy-related defects associated with the *opi3Δ* mutant.

In yeast, the Opi1 repressor plays an important role in the regulation of PL biosynthetic gene expression, such as *INO1* and *CHO2*. Prior studies established that PA with short acyl chains was a determinant factor in the binding of Opi1p to the ER membrane, in association with the Scs2 protein, to de-repress PL genes during growth in inositol limiting conditions (Hofbauer et al., 2014). Here we found that an increased accumulation of PA 32:1, relative to that measured in WT yeast, is closely associated with GPI-AP secretion and to the manifestation of many additional phenotypes in the *opi3Δ* mutant. In contrast, abrogation of the *opi3Δ* mutant pleiotropic phenotypes strongly correlated with a reduced content of PA 32:1 and a concomitant increased abundance of PA 34:2 in *opi3Δ gut2Δ* and *opi3Δ gpp2Δ* double mutants. The MAPK/Hog1 signaling pathway was found to be activated in the *opi3Δ* mutant during growth in inositol limiting conditions. Combined with the up-regulation of Gut2p in this mutant, glycerol production triggered by activated MAPK/Hog1 suggests a mechanism explaining its increased PA 32:1 levels. By increasing the DHAP/Gro-3-P ratio, acylation of DHAP by the Gpt2p lessens its availability for Gro-3-P acylation leaving Sct1p, with a net preference for Gro-3-P and C16 acyl chains, the main contributor for the pool of PA derived from Gro-3-P (Fig. 7; *opi3Δ*). Hence, while this study confirms that the relative abundance of PA with short acyl chains correlates with PL gene transcription, activation of the MAPK/Hog1 pathway defines a mechanism quite distinct from the Snf1p-regulated Acc1 activity previously described (Hofbauer et al., 2014).

In contrast to that previously reported for WT yeast growing in inositol limiting conditions (Hofbauer et al., 2014; Loewen et al., 2004), the bulk of GFP-Opi1 in the *opi3Δ* mutant is bound to punctate structures rather than to the typical ring-like shape fluorescent staining resulting from binding of the repressor to PA and Scs2p at the perinuclear ER membrane/nuclear envelope (Fig. 7; *WT vs opi3Δ*). In line with previous reports, these fluorescent puncta were present at sites of LD

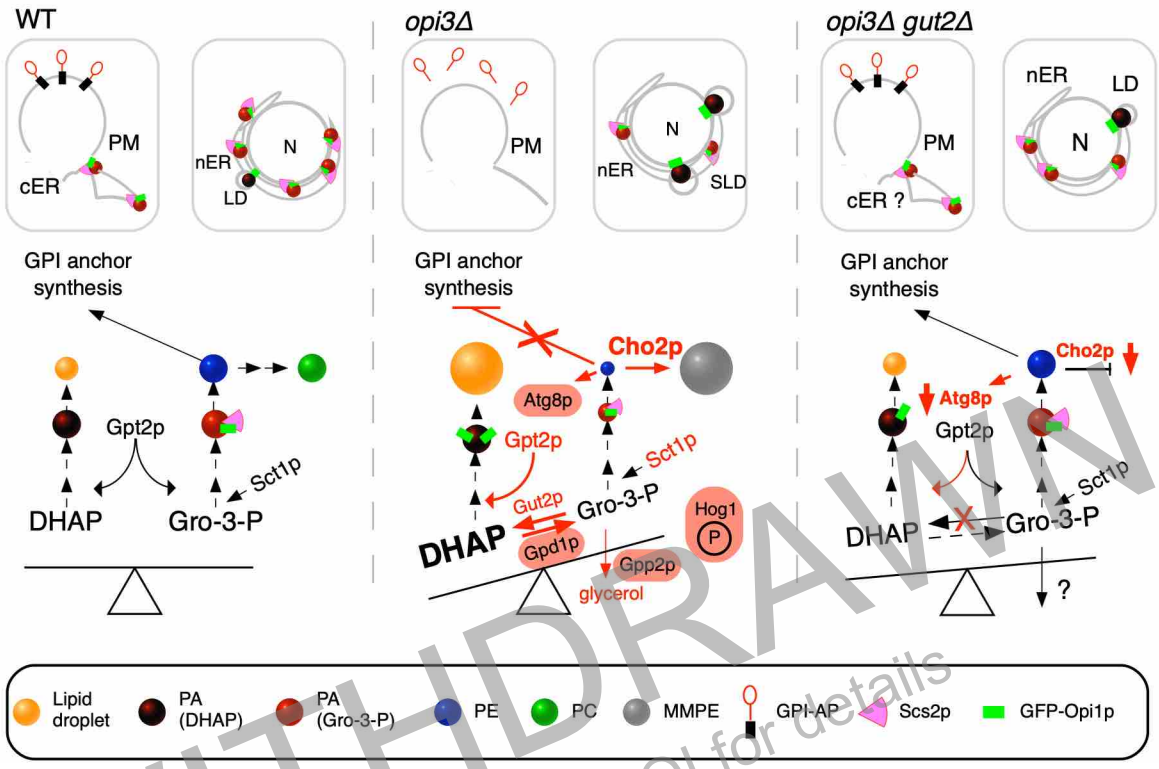




**Figure 7. Proposed models for the implication of the MAPK/Hog1 pathway in the *opi3Δ* mutant and the abrogation of its pleiotropic phenotypes by the deletion *GUT2***

formation (Gaspar et al., 2017; Romanauska and Kohler, 2018), often hypertrophied (SLD) in the *opi3Δ* mutant (Fig. 5B; Fig. S5). Binding of GFP-Opi1 to these structures could only be detected in the absence of Opi1p/Scs2p interaction (*i.e. scs2Δ* mutant or WT yeast expressing GFP-Opi1p lacking the the Scs2-interacting domain) and in the absence of inositol and choline in the medium (Gaspar et al., 2017). These conditions are met when the *opi3Δ* mutant is grown in SC medium. Under these conditions, the PC level detected in the *opi3Δ* mutant was reduced by >150-fold and the Scs2 protein content was decreased by ~1.45 $\log_2$ compared to that found in WT yeast (Thibault et al., 2012). Scs2p is one of several tethers involved in maintaining cER/PM contact sites (Manford et al., 2012). The *scs2Δ* mutant is also a mild inositol auxotroph that can be corrected by interrupting PC synthesis from the Kennedy pathway or by stimulating its degradation by overexpression of a specific phospholipase b (Nte1) (Fernandez-Murray et al., 2009). Interestingly,

hypersaline stress, a condition that activates the MAPK/Hog1 pathway, is a potent inducer of PC degradation (Kiewietdejonge et al., 2006). As depicted in Fig. 7, our results support the view that activation of the MAPK/Hog1 pathway in response to inositol limitation favors the accumulation of a distinct pool of PA, derived from acylation of DHAP by Gpt2p, that forms localized puncta. Binding of GFP-Opi1 to this pool of PA would be Scs2p-independent, but largely affected by the PC content within the ER membrane hence explaining their abundance in the *opi3Δ* mutant. Closely associated with LD formation, this DHAP-derived PA pool appears to be preferentially and rapidly converted into TAG. This would account for the accumulation of PA with short acyl chains produced by the acylation of Gro-3-P by Sct1p.

Best known for its role in the high osmolarity glycerol response (Brewster et al., 1993), sustained activation of the MAPK/Hog1 pathway in the *opi3Δ* mutant is consistent with the prior finding that GPI anchor synthesis blocked either at the Mcd4, Gpi13 or Las21 steps constitutively activates this pathway (Toh-e and Oguchi, 2001). This is also in agreement with the implication of this pathway at a late stage of ER stress to help the UPR pathway restoring ER homeostasis (Bicknell et al., 2010). One of its role in ER stress is to stabilize the Atg8 protein and to induce autophagy upon tunicamycin treatment (Bicknell et al., 2010). As recently reported, Atg8p is also involved in a novel cell process known as microlipophagy. This process, identified in a mutant (*cho2Δ*) defective in PC synthesis, removes excess ER membranes aggregates by targeting lipid droplet for their degradation into the vacuole (Vevea et al., 2015). Hence, this suggests that in the context of the *opi3Δ* mutant phosphorylated MAPK/Hog1p stimulates both LD biogenesis, through DHAP-derived PA conversion into TAG, and their targeted degradation into the vacuole. Unlike the situation in the *cho2Δ* mutant however, the stimulation of PL gene expression (*CHO2*) combined with lipidation of an increased amount of Atg8p, exacerbate the shortage in PE, resulting in GPI anchor synthesis defect and secretion of GPI-APs in the *opi3Δ* mutant (Fig. 7; *opi3Δ*). This explains

its exquisite sensitivity to rapamycin treatment compared to the *cho2Δ* mutant (Fig. S8). Consistently, this also provides an example of a stress response trapped in a futile loop that perpetuates the conditions (ER stress) that initially triggered its implication to alleviate the primary stress.

Rewiring the three-carbon metabolism by deleting the *GUT2* or *GPP2* genes in the *opi3Δ* mutant was found to abrogate most of its phenotypes: the secretion of GPI-APs, the absence of GFP-Opi1 at the cell periphery, upregulation of Atg8p and the formation of SLD (Fig. 7; *opi3Δ gut2Δ*). This was associated with a significant decrease in PA 32:1 and a concomitant increase in PA 34:2 that correlated with a reduction in *INO1* gene expression and the nearly complete absence of Cho2-derived conversion of PE into MMPE. It is unclear from our results whether the striking improvement observed in these double mutants is limited to the repression of PL gene transcription by the Opi1 repressor. For instance, given the preference of Cho2p for PE 32:2 (Boumann et al., 2004; Boumann et al., 2003), the accumulation of MMPE in the *opi3Δ* might be partly driven by an excessive accumulation of PA with short acyl chains in this mutant. Also, the mitochondrial GPD encoded by *GUT2* is part of the Gro-3-P shuttle whose main function is to re-oxidize NADH into NAD+ (Mracek et al., 2013). NAD+ being an essential cofactor in the Ino1-catalyzed conversion of glucose-6-phosphate into inositol-1-phosphate (Chen and Charalampous, 1966; Geiger and Jin, 2006; Stein and Geiger, 2002), the limiting reaction in the formation of *myo*-inositol, it is possible that disrupting the Gro-3-P shuttle affects this enzymatic reaction.

The *pemt*$^{-/-}$ deficient mice develop hepatic steatosis due to a reduced PC/PE ratio (Li et al., 2006) and PEMT insufficiency has been reported as a risk factor for human lean nonalcoholic steatohepatitis (Nakatsuka et al., 2016). *pemt*$^{-/-}$ deficient mice were also found to be protected against diet-induced obesity, insulin resistance and T2D whereas WT animals were not (Jacobs et

al., 2010). Because the *cho2Δ* and *opi3Δ* yeast mutants are similarly characterized by decreased PC/PE ratios, they have been considered as a unicellular model for this liver disease (Thibault et al., 2012). However, because all three methylation steps converting PE into PC are catalyzed by PEMT in mammals its deletion, by analogy with the yeast *cho2Δ* mutant, would not cause a shortage in PE and thus would be predicted not to affect GPI anchor synthesis. Conversely, overexpression of PEMT, which is associated with greater risks of obesity and T2D, might do so (Fu et al., 2011; Sharma et al., 2013). That shortage in PE, and consequent loss of GPI-AP stability, might be linked with these pathologies is supported by the finding that mice deficient in the PCYT2 gene, encoding the CTP-phosphoethanolamine cytidyl transferase involved in PE synthesis, are obese and insulin resistant (Singh et al., 2012). In contrast, single nucleotide polymorphisms associated with its overexpression are negatively correlated with percent fat mass and body mass index (Sharma et al., 2013). A direct predicted consequence of GPI anchor synthesis deficiency, in addition to the release of GPI-APs, is the build-up within the ER membrane of immature GPI anchors. Given the established role of the GPI-specific phospholipase D (GPLD1) in GPI anchors hydrolysis (Mann et al., 2004; Roberts et al., 1988; Toutant et al., 1989), this might explain why its overexpression is a biomarker in T2D (Sanjabi et al., 2015; von Toerne et al., 2016). Of note, one of the most upregulated protein in the *opi3Δ* mutant (mean log2 = 5.02) is encoded by the uncharacterized ORF YJL132W which shows homology with mammalian GPLD1 (Thibault et al., 2012).

The analogy between animal models of T2D and the "obese" yeast *opi3Δ* mutant also extends to the possible mechanism of action of some anti-glycemic drugs. Metformin, the most prescribed anti-glycemic drug for T2D patients over the past 50 years, was reported to inhibit, directly or not, mGPD function, the ortholog of yeast Gut2p (Madiraju et al., 2014; Madiraju et al., 2018). This

was associated with an increased cytosolic NADH/NAD+ ratio, expected for disruption of the Gro-3-P shuttle, and a reported reduction in hepatic gluconeogenesis and plasma levels of glucose at resting state. Whether mGPD is a direct or indirect metformin target is controversial (Calza et al., 2018). Nonetheless, disrupting mGPD expression, either transiently in the rat animal model or in mGPD KO mice, phenocopied these observations (Madiraju et al., 2014). Furthermore, in an animal model of T2D, modification of cytosolic redox status was reported to be the main mode of action of metformin (Madiraju et al., 2018). Another postulated target of metformin is AMPK, the energy sensor kinase whose homolog in yeast is Snf1p. Both metformin and the AMPK activator AICAR were shown to protect against palmitate-induced apoptosis (Dai et al., 2015; Eriksson and Nystrom, 2014), a condition associated with elevated malonyl-CoA levels in the diabetic state, in part by attenuating phosphorylation of p38 MAPK, an ortholog of the yeast Hog1p. In yeast, activation of Snf1p was also shown to act as a negative regulator of Hog1p activation during ER stress (Mizuno et al., 2015). Hence, the intricate connection between Hog1p activation, cellular dysfunction and the central metabolism elucidated in the present study might be relevant to chronic diseases in humans.



In conclusion, we have shown here that membrane raft integrity is compromised in a yeast model of metabolic disorder associated with lipid imbalance. This is consequent to the sustained activation of the MAPK/Hog1 signaling pathway that promotes upregulation of PL biosynthesis and causes shortage of PE for GPI anchor synthesis. Deletion of either *GUT2* or *GPP2* counteracts activation of this stress pathway by reducing the DHAP/Gro-3-P ratio. This restores GPI-APs attachment to membranes, normal growth and prevents LD hypertrophy.

## ACKNOWLEDGEMENTS

The authors are in debt with C. Landry (Université Laval) who gave us access to several of his equipment facilities, H. Riezman (University of Geneva) who generously provided the Gas1 antiserum and V. Siewers and F. David (Technical University of Denmark) for plasmid pFDA09. The authors would also like to thank H. Deveau and students from the laboratory course BCM-3010 (Université Laval) for the yeast *opi3Δ::NAT ERG6*-mCherry*::HYG* strain construct and I. Gagnon-Arsenault (Université Laval) for her critical comments on the manuscript. This work was supported by grants from the Natural Sciences and Engineering Research Council of Canada (RGPIN/05191-2014) and from Le *Fonds* d'enseignement et de recherche de la Faculté des sciences et de génie, Université Laval (FO517704) awarded to Y.B. A grant from the Fonds de recherche du Québec-Santé (35048) and awarded to S. Charette partly supported F.L. V.I.T. was supported by grants from the Natural Sciences and Engineering Research Council of Canada (RGPIN 2014-04482 and CRDPJ 515900 - 17). K.M. was supported by the Concordia University Armand C. Archambault Fellowship and the Concordia University Dean of Arts and Sciences Award of Excellence. A.P. was supported by the Canadian Institutes of Health Research Frederick Banting and Charles Best Canada Master's Scholarship Award.



## AUTHOR CONTRIBUTIONS

A.K.D., N.M., F.L., A.P. and K.M. conducted and analyzed the data of most experiments. M.B., F.B. and F.L-G. contributed to experiments. Y.B. wrote the manuscript with the contribution of A.K.D, N.M., F.L., K.M. and V.I.T. A.K.D. and V.I.T. supervised parts of the project and Y.B conceived and supervised the study.

## DECLARATION OF INTERESTS

The authors declare that they have no competing interests.

# STAR Methods

## RESOURCE AVAILABILITY

### Lead Contact

Further information and requests for resources and reagents should be directed to and will be fulfilled by the Lead Contact, Yves Bourbonnais (Yves.Bourbonnais@bcm.ulaval.ca).



## EXPERIMENTAL MODEL AND SUBJECT DETAILS

### Yeast strains and media

The yeast trains used in this study are described in the Key Resources Table. All the strains are derived from BY4741 (MAT*a his3Δ1 leu2Δ0 met15Δ0 ura3Δ0*) except the ts mutants which are derived from the S288C strain genetic background. Gene deletion to produce double mutants were all constructed by standard PCR-based strategies to amplify resistance cassettes with appropriate flanking sequences and replacing the target gene by homologous recombination (Gardner and Jaspersen, 2014). For the *opi3Δ ERG6::*mCherry strain, the PCR fragment containing the mCherry coding sequence from plasmid pBS35 was inserted at the C-terminal end of the *ERG6* coding sequence. All constructed strains and genetic manipulations were confirmed by PCR.

In pilot experiments, yeast strains derived from the BY4742 genetic background (MAT*α his3Δ1 leu2Δ0* l*ys2Δ0 ura3Δ0*) were shown not to secrete GPI-APs upon *OPI3* deletion. However, this was not due to their mating type because strains derived from W303-1a or W303-1b (MATa/MATα (*leu2-3,112 trp1-1 can1-100 ura3-1 ade2-1 his3-11,15*) carrying the *opi3Δ* mutation secreted similar amounts of GPI-APs (Fig. S9).

Media used in this study were YPD (1% yeast extract, 2% bio-tryptone, 2% glucose) and SC (0.674% yeast nitrogen base (YNB; Bioshop Canada) without amino acids with ammonium sulfate, 2% glucose, 1.34 g/L of complete drop-out mix) pH 3.0 and 6.0 (containing a final concentration

of 50 mM of succinic acid; adjusted with 10N NaOH). SC medium used in inositol-related experiments had the same composition as SC except that YNB-inositol (MP Biomedicals, LLC) replaced the nitrogen base. For strains expressing plasmids, the drop out mix in SC was replaced by 1.27 g/L of a drop out mix without uracil.

**Plasmid construction**

Plasmids used in this study were previously described and are listed in KEY RESOURCES.

**METHOD DETAILS**

**Screening procedure**

The yeast knock-out collection (YKO) of non-essential genes was bought from Invitrogen (Mat-A Complete Set; Cat. no. 95401.H2). Each day 4 different plates from the YKO collection were thawed and used to inoculate 4 new 96 plates filled with 250 µl of SC media. For each well, 5 µl from the glycerol stock was transferred in the fresh media. The newly inoculated plate was incubated at 30°C without agitation for 48 h. On each plate column 2 was replaced with 2 replicates of 4 different control strains: BY4741 (WT), *gas1Δ*, *yps1Δ* and *kex2Δ*. After incubation, the plates were spined down and 200 µl of the supernatant was transferred by aspiration using an in-house device for dot-blot to a polyvinylidene difluoride membrane activated in methanol (PVDF; Pall Corporation). The PVDF membrane was then incubated in 10% skim milk (w/v) –TBST (20 mM Tris pH 7.6, 137 mM NaCl, 0.1% Tween 20) for 1 h. After dilution of the skim milk solution to 1%, using fresh TBST, immunodetection of Gas1p was performed using a rabbit Gas1 antiserum (Horvath et al., 1994) (1/10 000 final dilution), kindly provided by Howard Riezman (University of Geneva) for 1 h. After washes, 3 times 5 min with 1% skim milk-TBST solution, the membrane was incubated in 1% skim milk with 1:10 000 dilution of a goat anti-rabbit antibody coupled with the horseradish-perodixase system (1/10 000 final dilution; Sigma-Aldrich) for 1 h. Following the

secondary antibody incubation, the signal was revealed with an ECL reagents kit (Amersham) on an Amersham hyperfilm ECL (Amersham). The intensity of each spot was analyzed using the software GeneTools (Syngene). Subsequent rounds were performed as round one, except that we used a rabbit anti-Yps1 serum (294-3; (Ash et al., 1995)) at a final dilution of 1/10 000 for immunodetection. Classification of the retained mutants (*see Quantification and Statistical Analysis*) according to the estimated molecular weight of the major Yps1p isoforms secreted was done by Western blotting (*see below*) with yeast transformants carrying the engineered single chain Yps1p polypeptide derived from pRS426-YPS1-DL (Dube et al., 2015). Yeast transformations were performed by the lithium acetate procedure described by (Gietz and Woods, 2002).



**Protein extracts, SDS-PAGE and Western blots**

- Model GPI-APs (Yps1p and Gas1p)

Cells were pre-cultured in SC medium (buffered at pH 6.0 throughout, except for the initial screening procedure described above) overnight to stationary phase and then diluted at 0.1 $OD_{600}$ unit in fresh medium (in an Erlenmeyer containing 1/5 of its maximal volume capacity). The cultures were then further incubated at 30°C for 24 h. At the end of the incubation, a volume equivalent to 10 $DO_{600}$ units was spin for the preparation of total protein extract (*see* below). The cleared supernatant from the remaining of each culture was concentrated, as described previously (Gagnon-Arsenault et al., 2008), on an Amicon Ultra 10 KDa membrane (Millipore) with multiple spins at 1400 x g (4°C) until the initial volume was concentrated at least 100-fold. The residual volume was precisely measured and an equivalent of 5 $OD_{600}$ units was processed for SDS-polyacrylamide gel electrophoresis (PAGE), the remaining being conserved at -20°C until further use.

Total protein extracts were prepared from cell pellets (equivalent to 10 $DO_{600}$ units) as described in (Ash et al., 1995). An equivalent of 0.5 $OD_{600}$ unit was used for SDS-PAGE analysis, the

remaining was conserved at -20°C. In some experiments, concentrated supernatants and cell extracts were first treated with Endo $H_f$ (New England Biolabs) prior to SDS-PAGE to reduce heterogeneity caused by *N*-linked oligosaccharides. This was carried out according to the manufacturer's brochure using 100 U of Endo $H_f$ per sample, in total volume of 20 µL, and an incubation at 37°C for 2 h.

For GPI-APs immunodetection, an equivalent of 0.5 $OD_{600}$ unit of intracellular total protein extracts was deposited per lane for gel electrophoresis compared to 5.0 $OD_{600}$ units for the concentrated supernatants (10-fold) to facilitate detection of the small amount of GPI-AP secreted by WT and the *opi3Δ* positive modifiers. The loading buffer for SDS-PAGE analysis was supplemented (Yps1p) or not (Gas1p) with 100 mM DTT. Electrophoresis was carried out on 10 % polyacrylamide gels at 175 V for 1 h using the Mini-PROTEAN Tetra Cell unit (Bio-Rad) and Power Supply (Model EC250-90l; EC Apparatus Corp.). Gels were then transferred onto nitrocellulose membranes (Mandel) for 1 h 10 at 34 mA/gel (transfer buffer; 20% methanol, 24.2 mM Tris-Base, 192 mM glycine) with a semi-dry transfer unit (Amersham Biosciences (SF) Corp.) and placed overnight in Odyssey Blocking Buffer (PBS) (LI-COR Biosciences). For immunodetection, the membranes were incubated for 2 h in the same buffer, supplemented with 0.001% Tween 20, with either a rabbit anti-Yps1 antiserum (α-294-3/4 used at 1:10 000 dilution for native Yps1p (Ash et al., 1995) or α-268-6 used at 1:5 000 dilution for Yps1-DL (Dube et al., 2015)) or a rabbit anti-Gas1 antiserum (1:5 000 final dilution). In all GPI-AP immunoblots actin was used as a loading control and a mouse anti-α-actin antiserum (1: 5 000 final dilution) was also added. Following two washes (7.5 min each) with PBST (PBS supplemented with 0.1% Tween 20) IRDye® 800CW Goat anti-Rabbit IgG and IRDye 680LT Goat anti-Mouse IgG secondary antibodies (each used at a 1:5 000 final dilution) were added in PBS and the membranes were

incubated for 1 h. After another washing step with PBST, the membranes were imaged by an Odyssey® Fc Imaging System (LI-COR Biosciences).

- Phosphorylated Snf1p and MAPK/Hog1p

Yeast cells were pre-cultured in SC medium pH 6.0 overnight to stationary phase and then diluted to 0.1 $OD_{600}$ unit/mL in a 250 mL Erlenmeyer containing 50 mL of fresh SC medium. The cultures were brought to log phase (between 0.5 and 1 $OD_{600}$ unit) and 25 mL were filtered on a 0.45 µM nitrocellulose filter. The cells were scrapped, immediately put into 1 mL of cold methanol and conserved in –80°C, as described by (Treitel et al., 1998), until cell extraction. As a positive control for phosphorylated Snf1, log phase cultures were shifted to SC medium containing 0.05% glucose for 30 min prior the filtration. The other 25 mL of culture was further incubated until stationary phase (24 h) and were treated as the log phase samples. For the negative Snf1 phosphorylation control, cultures were either shifted to fresh SC medium or glucose alone was added (final concentration of 2%) for 30 min, prior to the filtration. Total protein extraction was performed as described above for GPI-APs, except except that PhosSTOP (0.1 mg/mL; Roche Life Science) was added to the lysis solution. An equivalent of 0.5 $OD_{600}$ unit of cultures was loaded per lane for the SDS-PAGE. For the Western blots, the membranes were incubated with a rabbit anti-Phospho-AMPKα (anti-AMPK ; 1: 5 000 final dilution) or a goat anti-Snf1 (1: 5 000 final dilution) for 2 h followed by an incubation with IRDye® 800CW Goat anti-Rabbit IgG (1: 5000 final dilution) or with an IRDye 680RD Donkey-anti-Goat IgG for 1h. After washes, membranes were imaged as described above for GPI-APs with the Odyssey® Fc Imaging System (LI-COR Biosciences).

Dual phosphorylation of MAPK/Hog1p was assessed from early log phase cultures (between 0.5 and 1 $OD_{600}$ unit/ mL), prepared as described above, of yeast strains carrying the *HOG1::GFP*. BY4741 carrying the wild type *HOG1* allele and an *hog1Δ* mutant were also used as controls. The Hog1 phosphorylation positive controls were incubated 5 min with 0.5 M NaCl prior to protein

extraction carried out as described above for Snf1p. Protein extracts equivalent to 1 $OD_{600}$ unit were deposited per lane for SDS-PAGE analysis. Western blotting and detection was performed as above (Snf1p) but with a rabbit anti-Phospho p38 MAPK (1: 5 000 final dilution) or a rabbit anti-GFP (1: 5 000 final dilution) as primary antibodies.

- GFP-ATG8

Yeast strains transformed with plasmid pGFP-ATG8 (generously donated by DJ Klionsky; (Guan et al., 2001)) using the modified lithium acetate procedure (Gietz and Woods, 2002) were cultured in SC-ura medium until stationary phase. Protein extracts, equivalent to 1 $OD_{600}$ unit and prepared as described for GPI-APs, were deposited per lane for SDS-PAGE analysis. Western blotting was carried as described above using a rabbit anti-GFP antiserum. The loading control used was a non-specific band of ~54 kDa reacting with the rabbit anti-GFP primary antibody (Fig. S8).



**Malonyl-CoA sensor assay**

Yeast strains were transformed with the plasmid pFDA09 (generously provided by V. Siewers and F. David, Denmark;(David et al., 2016)) . Transformed strains were inoculated in 5 mL SC-leu media in a 13 mL snap-cap tube for 24 h. Yeast strains were next diluted to 0.15 $OD_{600}$/mL in fresh SC-leu media (5 mL) in 13 mL snap-cap. Early log phase cultures ($OD_{600}$ /mL between 0.5-0.7) were then supplemented with 13.5 µM of cerulenin and further incubated for 2 h. These cultures were then diluted 1:10 in 250 µl, and analyzed with a flow cytometer (Guava easyCyte HT) for 5000 recorded events. Fluorescence signal was read in 16 different channels, but we focused only on the Green-B channel for GFP. The rest of the 5 ml cultures were further incubated until stationary phase (18 h). As for the log phase cultures, 13.5 µM of cerulenin was added 2 h prior to flow cytometry analysis carried out with 1/100 diluted samples.

**Live-Cell Imaging of Yeast**

- Nile Red and BODIPY staining

Yeast cells were cultured to stationary phase in SC medium and then incubated with Nile red for 30 min, as described by (Fei et al., 2011) or with BODIPY 493/503. The pictures were taken with Axio Observer.Z1 microscope under a 63 X oil-immersion objective lens with a final magnification of 630 X. Cells were immediately visualized on fresh slides with an YFP (Nile Red) or GFP filters (BODIPY).

- GFP-Opi1p reporter

Yeast strains expressing the GFP-Opi1 plasmid were brought to log phase (between 0.5 and 1 $OD_{600}$ unit/ mL) in SC-URA medium and were immediately visualized as described above with the GFP filter. For the co-localization of GFP-Opi1p (GFP filter) and Erg6-mCherry (Texas Red filter) the *opi3Δ ERG6::*mCherry strain was grown to stationary phase in SC medium.



**Lipidomic analysis**

- Sample preparation

Yeast strains were inoculated in 5 mL SC complete media in 13ml snap-cap tube for 24h. Next day $OD_{600}$ was read and strains were diluted back at 0.15 in 50ml SC complete media in 250 mL Erlenmeyer for another 24h. Third day, $OD_{600}$ was read and equivalent of 5U OD600 was spined down. Supernatant was removed and pellet washed once with ice cold 0.155 M ammonium bicarbonate. Resuspended pellets were spined and supernatant remove. Pellets were then placed at -80°C until lipid extraction.

- Lipid extraction

The cell pellet was thawed on ice and then resuspended in 200 µl of ice-cold nanopure water. The cell suspension was transferred to a 15-ml high-strength glass screw-top centrifuge tube with a

polytetrafluoroethylene-lined cap. The following was added to this tube: 1) 25 µl of the mixture of internal lipid standards prepared in chloroform/methanol (2:1) mixture, 2) 100 µl of 425–600 µm acid-washed glass beads, and 3) 600 µl of chloroform/methanol (17:1) mixture. The tube was vortexed at high speed for 5 min at room temperature (RT) to disrupt the cells. The tube was then vortexed at low speed for 1 h at RT to facilitate lipids extraction. The sample was incubated for 15 min on ice to promote protein precipitation and the separation of the aqueous and organic phases from each other. The tube was centrifuged in a clinical centrifuge at 3,000 × g for 5 min at RT to facilitate the separation of the upper aqueous phase and the lower organic phase, which contained all lipid classes. A borosilicate glass pipette was used to transfer the lower organic phase (~400 µl) to another 15-ml high-strength glass screw-top centrifuge tube with a polytetrafluoroethylene-lined cap. The lower organic phase was kept under the flow of nitrogen gas. 300 µl of chloroform-methanol (2:1) mixture was added to the remaining upper aqueous phase to allow the extraction of sphingolipids and phosphatidic acid, phosphatidylserine, phosphatidylinositol and cardiolipin. The tube was vortexed vigorously for 5 min at RT and then centrifuged in a clinical centrifuge at 3,000 × g for 5 min at RT. A borosilicate glass pipette was used to transfer the lower organic phase (~ 200 µl) formed after centrifugation to the organic phase collected at the previous step. The solvent in the combined organic phases was evaporated under the flow of nitrogen gas. The tube containing the lipid film was closed under the flow of nitrogen gas and then stored at -80 °C.



- Mass spectrometry (MS) analysis

500 µl of acetonitrile (ACN)/2-propanol/nanopure water (65:35:5) mixture was added to a tube containing the lipid film stored at -80 °C, and the tube was vortexed 3 times for 10 s at RT. The tube's content was subjected to ultrasonic sonication for 15 min, and the tube was vortexed again 3 times for 10 s at RT. 100 µl of a sample was taken from the tube and added to a glass vial with an insert used for a wellplate. A liquid chromatography (LC) system was used to separate different

lipid species on a reverse-phase C18 column CSH coupled to a pre-column system. During lipid separation, the column was maintained at 55 °C and a flow rate of 0.3 ml/min, and the sample was kept in the wellplate at RT. The mobile phases that consisted of mixture A (ACN/water [60:40 (v/v)]) and mixture B (isopropanol/ACN [90:10 (v/v)]) were used for the chromatographic separation of lipids. For a positive mode of detecting parent ions created using the electrospray ionization (ESI) ion source, the ESI (+) mode, the mobile phases A and B contained ammonium formate at the final concentration of 10 mM. For a negative mode of parent ions detection, the ESI (-) mode, the mobile phases A and B contained ammonium acetate at the final concentration of 10 mM. A sample volume of 10 µl was used for the injection in both the ESI (+) and ESI (-) modes. Different lipid species were separated by LC using the following LC gradient: 0–1 min 10% (phase B); 1–4 min 60% (phase B); 4–10 min 68% (phase B); 10–21 min 97% (phase B); 21–24 min 97% (phase B); 24–33 min 10% (phase B). Extraction blanks were run as the first sample, between every four samples, and as the last sample. The background was subtracted to normalize data. A Thermo Orbitrap Velos mass spectrometer equipped with a HESI (heated electrospray ionization) ion source was used to analyze lipids separated by LC. The settings used for such analysis are provided in Table 1. The Fourier transform analyzer was used to detect parent ions (MS1) at a resolution of 60,000 and within the mass range of 150–2,000 Da. The settings shown in Table 2 were used to detect secondary ions (MS2). The Lipid Search software (V4.1; Fisher Scientific) was used to identify and quantify different lipids from raw LC-MS/MS files. This software uses the largest lipid database, containing more than 1.5 million lipid ion precursors (MS1) and their predicted fragment ions (MS2). The software also uses MS1 peaks for lipid quantitation and MS2 for lipid identification. LC-MS raw files containing full-scan MS1 data and data-dependent MS2 records were searched for free (unesterified) fatty acids (FFA), cardiolipin (CL), monomethyl-phosphatidylethanolamine (MMPE), phytoceramide (PHC), phytosphingosine (PHS),

phosphatidylcholine (PC), phosphatidylethanolamine (PE), phosphatidylglycerol (PG), phosphatidylinositol (PI), phosphatidylserine (PS), and triacylglycerol (TAG) lipid classes. The m/z tolerance values of 5 ppm and 10 ppm were used for MS1 and MS2 ions. Other search parameters are provided in Table 3.

**Table 1. The settings used for mass spectrometric analysis of lipids separated by LC.**

Abbreviation: HESI, heated electrospray ionization.

| | |
|---|---|
| FTMS + p resolution | 60000 |
| Mass range (dalton) | 150-2000 |
| Ion source type | HESI |
| Capillary temperature (°C) | 300 |
| Source heater temperature (°C) | 300 |
| Sheath gas flow | 10 |
| Aux gas flow | 5 |
| Positive polarity voltage (kV) | 3 |
| Negative polarity voltage (kV) | 3 |
| Source current (µA) | 100 |



**Table 2. The settings for detecting MS2 ions with the help of the Fourier transform analyzer.**

| Instrument polarity | Positive | Negative |
|---|---|---|
| Activation type | High-energy-induced-collision-dissociation | Collision-induced-dissociation |
| Minimal signal required | 5000 | 5000 |
| Isolation width | 2 | 2 |
| Normalized collision energy | 55 | 35 |
| Default charge state | 2 | 2 |
| Activation time | 0.1 | 10 |
| FTMS + C resolution | 7500 | |
| 5 most intense peaks were selected for ms/ms | | |

**Table 3. The parameters used to identify and quantify lipids from the LC-MS raw files containing full-scan MS1 data and data-dependent MS2 records.**

| | |
|---|---|
| Identification | |
| Database | Orbitrap |
| Peak detection | Recall isotope (ON) |
| Search option | Product search Orbitrap |
| Search type | Product |
| Experiment type | LC-MS |
| Precursor tolerance | 10 ppm |
| Product tolerance | High-energy-induced-collision-dissociation [ESI (+) mode]: 20 ppm |
| | Collision-induced-dissociation [ESI (-) mode]: 0.5 Daltons |
| | |
| Quantitation | |
| Execute quantitation | ON |
| m/z tolerance | -5.0; +5.0 |
| Tolerance type | ppm |
| | |
| Filter | |
| Top rank filter | ON |
| Main node filter | Main isomer peak |
| m-score threshold | 5 |
| c-score threshold | 2 |
| FFA priority | ON |
| ID quality filter | A: Lipid class & all fatty acids are completely identified |
| | B: Lipid class & some fatty acids are identified |
| | C: Lipid class or FA are identified |
| | D: Lipid identified by other fragment ions (H2O, etc.) |
| | |
| Lipid Class | |
| High-energy-induced-collision-dissociation [ESI (+) mode] | PC, TAG |
| Collision-induced-dissociation [ESI (-) mode] | CER, CL, FFA, PE, PG, PI, PS |
| | |
| Ions | |

| | |
|---|---|
| High-energy-induced-collision-dissociation [ESI (+) mode] | + H; + NH4; + Na |
| Collision-induced-dissociation [ESI (-) mode] | - H; - 2H; - HCOO |

**Yeast growth assay**

Yeast strains were inoculated in 250 µL of SC medium in a 96-wells plate for 24 h at 30°C. Next day, $OD_{600}$ was read and yeast culture were diluted 3 µL in 250 µL of fresh SC media in a 96-wells plate. $OD_{600}$ of each well was followed using a TECAN plate reader with medium shaking at temperature and time indicated on each figure.



**Spotting assays**

Cells were pre-cultured in SC medium pH 6.0 overnight to stationary phase. A volume equivalent to 1 $OD_{600}$ unit, was spin and resuspended into 1 mL of sterile water. Aliquots (5 µL) of a series of 5-fold dilutions in sterile water (ND, 1/5, 1/25, 1/125, 1/625) were spotted on YPD or SC plates at the indicated temperature or on SC plates supplemented with either DMSO or DMSO plus 5 ng/mL Rapamycin. The plates were incubated for 3 d and pictures were taken.

**Opi− Phenotype**

The indirect measure of inositol secretion (Opi− assay) is based on the method developed by Hancock et al. (Hancock et al., 2006). Cells were cultured in SC medium pH 6.0 overnight to stationary phase. A volume equivalent to 1 $OD_{600}$ unit was spin down and the cell pellet resuspended in 1 mL of sterile water. From this cell suspension, 15 µL was streaked onto an SC-Inositol plate and incubated 3 d at 30ºC. At the end of the incubation, the reporter inositol auxotroph strain (*ino1Δ*), pre-cultured in SC medium pH 6.0 overnight to stationary phase, was similarly diluted into sterile water and 5 µL aliquots were streaked into three perpendicular lanes from the

Opi- phenotype testing strain using a template under the Petri dish. The plates were then incubated for another 3 d at 30ºC and pictures were taken. The relative secretion of inositol was estimated from the extent of growth of the *ino1Δ* auxotroph from triplicate biological samples of the various tester strains compared to that of BY4741 used as a negative control.

**qRT-PCR**

The glass bead mechanical procedure with the Invitrogen TRIzol and the Qiagen RNeasy mini kit were used to prepare total RNA preparation from log phase cultures (~ 1 OD unit/mL) of the yeast strains BY4741, *opi3Δ* and *opi3Δ gut2Δ*. After RQ1 DNAse (Promega) treatment of the purified RNA for 30 min at 37ºC, first strand cDNA synthesis was carried out at the same temperature for 50 min with Oligo $(dT)_{15}$ Primer (Promega) and Invitrogen M-MLV Reverse Transcriptase (Thermo Fisher Scientific). qRT-PCR with $F3_{act1}$ and $R3_{act1}$ and $F3_{ino1}$ and $R3_{ino1}$ primers (*see* KEY RESOURCES), first strand cDNA and iQ SYBR Green supermix (Bio-Rad) was performed for 40 cycles in a Bio-Rad Connect Thermocycler according the following scheme: 95 ºC 15 sec, 56 ºC 15 sec and 72 ºC 30 sec.



**QUANTIFICATION AND STATISTICAL ANALYSIS**

**Screening procedure**

Once all plates of the YKO collection following the first round with the Gas1 antiserum was done, a statistical correction (*B-score*; (Malo et al., 2006)) was applied to minimize position effects on the plate using the equation;

$$\text{B-score} = \frac{r_{ijp}}{MAD_p}$$

Where $r_{ijp}$ is the residual of the measurement for row $i$ and column $j$ on the plate $p$ and $MADp$ is the median absolute deviation.

Top ranking deletions (*B-score* value > 2; ~10% of all the YKO collection) were selected for a second round. Hit identification of round two was performed by comparing the spot intensity of each deletion to that of WT yeast. Deletions showing an increase of >1.5 fold for the shedding of Yps1p relative to that of WT yeast were selected for further analysis (71 mutants). To reduce position effects, different 96 well plates were then prepared and immunodetection for the release of Yps1p was again performed in triplicate. From the 71 mutants, 35 showed a statistical difference ($p < 0.05$; one-sided Student's t-test and/or Wilcoxon) compared to the WT.



**Western blots**

- GPI-APs (Yps1p and Gas1p)

The percentage of secreted GPI-APs was calculated from the signal intensities (SI) of the intracellular ($SI_i$) and extracellular material ($SI_e$) obtained with the Odyssey Imaging System from Western blots, taken into account that 10X more material was loaded for the extracellular material, and by correcting with the signal intensities of the loading controls ($SI_{lc}$) as follows:

$$\% \text{ GPI-APs (released)} = \frac{SI_e / SI_{lc}}{(SI_i / SI_{lc} \times 10) + SI_e / SI_{lc}} \times 100$$

- Phosphorylated MAPK/Hog1p

The relative amount of dually phosphorylated Hog1p was calculated by the ratio of the signal intensities obtained with the Odyssey Imaging System from identical aliquots of total protein extracts immunoblotted with the anti-p38 ($SI_{p38}$) and anti-GFP ($SI_{GFP}$) antisera as follows:

$$\text{Ratio} = \frac{SI_{p38}}{SI_{GFP}}$$

- GFP-Atg8p

The percentage of free GFP over the total GFP signal (GFP-Atg8 + GFP) was calculated with the Odyssey Imaging System from their respective signal intensities, $SI_{GFP}$ and $SI_{GFP\text{-}Atg8}$ from Western blots as follows:

$$\% \text{ Free Atg8p} = \frac{SI_{GFP}}{SI_{GFP} + SI_{GFP\text{-}Atg8}} \times 100$$

Quantification of total Atg8p was measured from the corresponding signal intensities of GFP and GFP-Atg8p as above from biological replicates loaded onto different western blots. This total intensity was then divided by the intensity of a non-specific ($SI_{NS\text{-}GFP}$) band (~54 kDa) reacting with the GFP antiserum enabling direct comparisons between the blots as follows:

$$\text{Total Atg8p} = \frac{SI_{GFP} + SI_{GFP\text{-}Atg8}}{SI_{NS\text{-}GFP}}$$



**Live-Cell imaging**

From stationary phase cultures of the various yeast strains, the percentage of cells with SLD was determined by visual inspection of the micrographs without template and tabulated in excel sheets. Two different experimentalists carried out the microscopic examination and counting for the Nile Red and BODIPY staining.

For the GFP-Opi1p distribution (punctate structures, perinuclear and cell periphery), micrographs were examined by two observers and the relative percentages assigned to the different structures did not exceed 13% between observers. One of these is shown in Fig. 5B. For the cell periphery (cER)/perinuclear (nER) fluorescent intensity ratios, this was done by freehand selection in Image Studio Lite of the area covering the cell periphery and the nucleus from micrographs of the different strains.

## qRT-PCR

The fold-change for the expression of *INO1* was determined by the ΔΔCq method from three biological replicates performed in duplicata.

Throughout the study, the Shapiro-Wilk normality test was used. Statistical analysis was done by a Student's t-test, for equal or unequal variance as first assessed by an F test, for samples conforming to the normal distribution or by the Wilcoxon rank sum test. Statistically significant difference was assigned for P-values < 0.05.



## REFERENCES

Ash, J., Dominguez, M., Bergeron, J.J., Thomas, D.Y., and Bourbonnais, Y. (1995). The yeast proprotein convertase encoded by YAP3 is a glycophosphatidylinositol-anchored protein that localizes to the plasma membrane. J Biol Chem *270*, 20847-20854.

Athenstaedt, K., Weys, S., Paltauf, F., and Daum, G. (1999). Redundant systems of phosphatidic acid biosynthesis via acylation of glycerol-3-phosphate or dihydroxyacetone phosphate in the yeast Saccharomyces cerevisiae. J Bacteriol *181*, 1458-1463.

Bicknell, A.A., Tourtellotte, J., and Niwa, M. (2010). Late phase of the endoplasmic reticulum stress response pathway is regulated by Hog1 MAP kinase. J Biol Chem *285*, 17545-17555.

Boslem, E., Weir, J.M., MacIntosh, G., Sue, N., Cantley, J., Meikle, P.J., and Biden, T.J. (2013). Alteration of endoplasmic reticulum lipid rafts contributes to lipotoxicity in pancreatic beta-cells. J Biol Chem *288*, 26569-26582.

Bosson, R., Jaquenoud, M., and Conzelmann, A. (2006). GUP1 of Saccharomyces cerevisiae encodes an O-acyltransferase involved in remodeling of the GPI anchor. Mol Biol Cell *17*, 2636-2645.

Boumann, H.A., Chin, P.T., Heck, A.J., De Kruijff, B., and De Kroon, A.I. (2004). The yeast phospholipid N-methyltransferases catalyzing the synthesis of phosphatidylcholine preferentially convert di-C16:1 substrates both in vivo and in vitro. J Biol Chem *279*, 40314-40319.

Boumann, H.A., Damen, M.J., Versluis, C., Heck, A.J., de Kruijff, B., and de Kroon, A.I. (2003). The two biosynthetic routes leading to phosphatidylcholine in yeast produce different sets of molecular species. Evidence for lipid remodeling. Biochemistry (Mosc) *42*, 3054-3059.

Brewster, J.L., de Valoir, T., Dwyer, N.D., Winter, E., and Gustin, M.C. (1993). An osmosensing signal transduction pathway in yeast. Science *259*, 1760-1763.

Brown, D.A., and Rose, J.K. (1992). Sorting of GPI-anchored proteins to glycolipid-enriched membrane subdomains during transport to the apical cell surface. Cell *68*, 533-544.

Cai, H., Cong, W.N., Ji, S., Rothman, S., Maudsley, S., and Martin, B. (2012). Metabolic dysfunction in Alzheimer's disease and related neurodegenerative disorders. Curr Alzheimer Res *9*, 5-17.

Calza, G., Nyberg, E., Makinen, M., Soliymani, R., Cascone, A., Lindholm, D., Barborini, E., Baumann, M., Lalowski, M., and Eriksson, O. (2018). Lactate-Induced Glucose Output Is Unchanged by Metformin at a Therapeutic Concentration - A Mass Spectrometry Imaging Study of the Perfused Rat Liver. Front Pharmacol *9*, 141.

Castillon, G.A., Watanabe, R., Taylor, M., Schwabe, T.M., and Riezman, H. (2009). Concentration of GPI-anchored proteins upon ER exit in yeast. Traffic *10*, 186-200.

Chen, I.W., and Charalampous, F.C. (1966). Biochemical Studies on Inositol: IX. d-INOSITOL 1-PHOSPHATE AS INTERMEDIATE IN THE BIOSYNTHESIS OF INOSITOL FROM GLUCOSE 6-PHOSPHATE, AND CHARACTERISTICS OF TWO REACTIONS IN THIS BIOSYNTHESIS. J Biol Chem *241*, 2194-2199.

Cherry, J.M., Hong, E.L., Amundsen, C., Balakrishnan, R., Binkley, G., Chan, E.T., Christie, K.R., Costanzo, M.C., Dwight, S.S., Engel, S.R., *et al.* (2012). Saccharomyces Genome Database: the genomics resource of budding yeast. Nucleic Acids Res *40*, D700-705.

Dai, Y.L., Huang, S.L., and Leng, Y. (2015). AICAR and Metformin Exert AMPK-dependent Effects on INS-1E Pancreatic beta-cell Apoptosis via Differential Downstream Mechanisms. Int J Biol Sci *11*, 1272-1280.

David, F., Nielsen, J., and Siewers, V. (2016). Flux Control at the Malonyl-CoA Node through Hierarchical Dynamic Pathway Regulation in Saccharomyces cerevisiae. ACS Synth Biol *5*, 224-233.

Dube, A.K., Belanger, M., Gagnon-Arsenault, I., and Bourbonnais, Y. (2015). N-terminal entrance loop of yeast Yps1 and O-glycosylation of substrates are determinant factors controlling the shedding activity of this GPI-anchored endopeptidase. BMC microbiology *15*, 50.

Eriksson, L., and Nystrom, T. (2014). Activation of AMP-activated protein kinase by metformin protects human coronary artery endothelial cells against diabetic lipoapoptosis. Cardiovasc Diabetol *13*, 152.

Fankhauser, C., and Conzelmann, A. (1991). Purification, biosynthesis and cellular localization of a major 125-kDa glycophosphatidylinositol-anchored membrane glycoprotein of Saccharomyces cerevisiae. Eur J Biochem *195*, 439-448.

Fei, W., Shui, G., Zhang, Y., Krahmer, N., Ferguson, C., Kapterian, T.S., Lin, R.C., Dawes, I.W., Brown, A.J., Li, P., *et al.* (2011). A role for phosphatidic acid in the formation of "supersized" lipid droplets. PLoS genetics *7*, e1002201.

Fernandez-Murray, J.P., Gaspard, G.J., Jesch, S.A., and McMaster, C.R. (2009). NTE1-encoded phosphatidylcholine phospholipase b regulates transcription of phospholipid biosynthetic genes. J Biol Chem *284*, 36034-36046.

Fiedler, K., Kobayashi, T., Kurzchalia, T.V., and Simons, K. (1993). Glycosphingolipid-enriched, detergent-insoluble complexes in protein sorting in epithelial cells. Biochemistry (Mosc) *32*, 6365-6373.

Flury, I., Benachour, A., and Conzelmann, A. (2000). YLL031c belongs to a novel family of membrane proteins involved in the transfer of ethanolaminephosphate onto the core structure of glycosylphosphatidylinositol anchors in yeast. J Biol Chem *275*, 24458-24465.

Franceschi, C., and Campisi, J. (2014). Chronic inflammation (inflammaging) and its potential contribution to age-associated diseases. J Gerontol A Biol Sci Med Sci *69 Suppl 1*, S4-9.

Fu, S., Yang, L., Li, P., Hofmann, O., Dicker, L., Hide, W., Lin, X., Watkins, S.M., Ivanov, A.R., and Hotamisligil, G.S. (2011). Aberrant lipid metabolism disrupts calcium homeostasis causing liver endoplasmic reticulum stress in obesity. Nature *473*, 528-531.

Fujita, M., Umemura, M., Yoko-o, T., and Jigami, Y. (2006a). PER1 is required for GPI-phospholipase A2 activity and involved in lipid remodeling of GPI-anchored proteins. Mol Biol Cell *17*, 5253-5264.

Fujita, M., Yoko, O.T., and Jigami, Y. (2006b). Inositol deacylation by Bst1p is required for the quality control of glycosylphosphatidylinositol-anchored proteins. Mol Biol Cell *17*, 834-850.

Gagnon-Arsenault, I., Parise, L., Tremblay, J., and Bourbonnais, Y. (2008). Activation mechanism, functional role and shedding of glycosylphosphatidylinositol-anchored Yps1p at the Saccharomyces cerevisiae cell surface. Mol Microbiol *69*, 982-993.

Gardner, J.M., and Jaspersen, S.L. (2014). Manipulating the Yeast Genome: Deletion, Mutation, and Tagging by PCR. In Yeast Genetics: Methods and Protocols, J.S. Smith, and D.J. Burke, eds. (New York, NY: Springer New York), pp. 45-78.

Gaspar, M.L., Chang, Y.F., Jesch, S.A., Aregullin, M., and Henry, S.A. (2017). Interaction between repressor Opi1p and ER membrane protein Scs2p facilitates transit of phosphatidic acid

from the ER to mitochondria and is essential for INO1 gene expression in the presence of choline. J Biol Chem *292*, 18713-18728.

Geiger, J.H., and Jin, X. (2006). The structure and mechanism of myo-inositol-1-phosphate synthase. Subcell Biochem *39*, 157-180.

Gietz, R.D., and Woods, R.A. (2002). Transformation of yeast by lithium acetate/single-stranded carrier DNA/polyethylene glycol method. Methods Enzymol *350*, 87-96.

Gonzalez, M., Goddard, N., Hicks, C., Ovalle, R., Rauceo, J.M., Jue, C.K., and Lipke, P.N. (2010). A screen for deficiencies in GPI-anchorage of wall glycoproteins in yeast. Yeast *27*, 583-596.

Greenberg, M.L., Reiner, B., and Henry, S.A. (1982). Regulatory mutations of inositol biosynthesis in yeast: isolation of inositol-excreting mutants. Genetics *100*, 19-33.

Grossmann, G., Malinsky, J., Stahlschmidt, W., Loibl, M., Weig-Meckl, I., Frommer, W.B., Opekarova, M., and Tanner, W. (2008). Plasma membrane microdomains regulate turnover of transport proteins in yeast. J Cell Biol *183*, 1075-1088.

Guan, J., Stromhaug, P.E., George, M.D., Habibzadegah-Tari, P., Bevan, A., Dunn, W.A., Jr., and Klionsky, D.J. (2001). Cvt18/Gsa12 is required for cytoplasm-to-vacuole transport, pexophagy, and autophagy in Saccharomyces cerevisiae and Pichia pastoris. Mol Biol Cell *12*, 3821-3838.

Hancock, L.C., Behta, R.P., and Lopes, J.M. (2006). Genomic analysis of the Opi- phenotype. Genetics *173*, 621-634.

Hendrickson, D.G., Soifer, I., Wranik, B.J., Kim, G., Robles, M., Gibney, P.A., and McIsaac, R.S. (2018). A new experimental platform facilitates assessment of the transcriptional and chromatin landscapes of aging yeast. Elife *7*.

Henry, S.A., Gaspar, M.L., and Jesch, S.A. (2014). The response to inositol: regulation of glycerolipid metabolism and stress response signaling in yeast. Chem Phys Lipids *180*, 23-43.

Hofbauer, H.F., Schopf, F.H., Schleifer, H., Knittelfelder, O.L., Pieber, B., Rechberger, G.N., Wolinski, H., Gaspar, M.L., Kappe, C.O., Stadlmann, J.*, et al.* (2014). Regulation of gene expression through a transcriptional repressor that senses acyl-chain length in membrane phospholipids. Dev Cell *29*, 729-739.

Hofmann, K. (2000). A superfamily of membrane-bound O-acyltransferases with implications for wnt signaling. Trends Biochem Sci *25*, 111-112.

Horvath, A., Sutterlin, C., Manning-Krieg, U., Movva, N.R., and Riezman, H. (1994). Ceramide synthesis enhances transport of GPI-anchored proteins to the Golgi apparatus in yeast. EMBO J *13*, 3687-3695.

Hummasti, S., and Hotamisligil, G.S. (2010). Endoplasmic reticulum stress and inflammation in obesity and diabetes. Circ Res *107*, 579-591.

Imhof, I., Flury, I., Vionnet, C., Roubaty, C., Egger, D., and Conzelmann, A. (2004). Glycosylphosphatidylinositol (GPI) proteins of Saccharomyces cerevisiae contain ethanolamine phosphate groups on the alpha1,4-linked mannose of the GPI anchor. J Biol Chem *279*, 19614-19627.

Jacobs, R.L., Zhao, Y., Koonen, D.P., Sletten, T., Su, B., Lingrell, S., Cao, G., Peake, D.A., Kuo, M.S., Proctor, S.D.*, et al.* (2010). Impaired de novo choline synthesis explains why phosphatidylethanolamine N-methyltransferase-deficient mice are protected from diet-induced obesity. J Biol Chem *285*, 22403-22413.

Jonikas, M.C., Collins, S.R., Denic, V., Oh, E., Quan, E.M., Schmid, V., Weibezahn, J., Schwappach, B., Walter, P., Weissman, J.S.*, et al.* (2009). Comprehensive characterization of genes required for protein folding in the endoplasmic reticulum. Science *323*, 1693-1697.

Kajiwara, K., Watanabe, R., Pichler, H., Ihara, K., Murakami, S., Riezman, H., and Funato, K. (2008). Yeast ARV1 is required for efficient delivery of an early GPI intermediate to the first mannosyltransferase during GPI assembly and controls lipid flow from the endoplasmic reticulum. Mol Biol Cell *19*, 2069-2082.

Kennedy, B.K., Berger, S.L., Brunet, A., Campisi, J., Cuervo, A.M., Epel, E.S., Franceschi, C., Lithgow, G.J., Morimoto, R.I., Pessin, J.E.*, et al.* (2014). Geroscience: linking aging to chronic disease. Cell *159*, 709-713.

Kennedy, E.P., and Weiss, S.B. (1956). The function of cytidine coenzymes in the biosynthesis of phospholipides. J Biol Chem *222*, 193-214.

Khurana, V., and Lindquist, S. (2010). Modelling neurodegeneration in Saccharomyces cerevisiae: why cook with baker's yeast? Nat Rev Neurosci *11*, 436-449.

Kiewietdejonge, A., Pitts, M., Cabuhat, L., Sherman, C., Kladwang, W., Miramontes, G., Floresvillar, J., Chan, J., and Ramirez, R.M. (2006). Hypersaline stress induces the turnover of phosphatidylcholine and results in the synthesis of the renal osmoprotectant glycerophosphocholine in Saccharomyces cerevisiae. FEMS Yeast Res *6*, 205-217.

Kinoshita, T., and Fujita, M. (2016). Biosynthesis of GPI-anchored proteins: special emphasis on GPI lipid remodeling. J Lipid Res *57*, 6-24.

Kodaki, T., and Yamashita, S. (1987). Yeast phosphatidylethanolamine methylation pathway. Cloning and characterization of two distinct methyltransferase genes. J Biol Chem *262*, 15428-15435.

Leidich, S.D., Drapp, D.A., and Orlean, P. (1994). A conditionally lethal yeast mutant blocked at the first step in glycosyl phosphatidylinositol anchor synthesis. J Biol Chem *269*, 10193-10196.

Li, Z., Agellon, L.B., Allen, T.M., Umeda, M., Jewell, L., Mason, A., and Vance, D.E. (2006). The ratio of phosphatidylcholine to phosphatidylethanolamine influences membrane integrity and steatohepatitis. Cell Metab *3*, 321-331.

Loewen, C.J., Gaspar, M.L., Jesch, S.A., Delon, C., Ktistakis, N.T., Henry, S.A., and Levine, T.P. (2004). Phospholipid metabolism regulated by a transcription factor sensing phosphatidic acid. Science *304*, 1644-1647.

Longo, V.D., Shadel, G.S., Kaeberlein, M., and Kennedy, B. (2012). Replicative and chronological aging in Saccharomyces cerevisiae. Cell Metab *16*, 18-31.

Lussier, M., White, A.M., Sheraton, J., di Paolo, T., Treadwell, J., Southard, S.B., Horenstein, C.I., Chen-Weiner, J., Ram, A.F., Kapteyn, J.C., *et al.* (1997). Large scale identification of genes involved in cell surface biosynthesis and architecture in Saccharomyces cerevisiae. Genetics *147*, 435-450.

Madiraju, A.K., Erion, D.M., Rahimi, Y., Zhang, X.M., Braddock, D.T., Albright, R.A., Prigaro, B.J., Wood, J.L., Bhanot, S., MacDonald, M.J., *et al.* (2014). Metformin suppresses gluconeogenesis by inhibiting mitochondrial glycerophosphate dehydrogenase. Nature *510*, 542-546.

Madiraju, A.K., Qiu, Y., Perry, R.J., Rahimi, Y., Zhang, X.M., Zhang, D., Camporez, J.G., Cline, G.W., Butrico, G.M., Kemp, B.E., *et al.* (2018). Metformin inhibits gluconeogenesis via a redox-dependent mechanism in vivo. Nat Med *24*, 1384-1394.

Malo, N., Hanley, J.A., Cerquozzi, S., Pelletier, J., and Nadon, R. (2006). Statistical practice in high-throughput screening data analysis. Nat Biotechnol *24*, 167-175.

Manford, A.G., Stefan, C.J., Yuan, H.L., Macgurn, J.A., and Emr, S.D. (2012). ER-to-plasma membrane tethering proteins regulate cell signaling and ER morphology. Dev Cell *23*, 1129-1140.

Mann, K.J., Hepworth, M.R., Raikwar, N.S., Deeg, M.A., and Sevlever, D. (2004). Effect of glycosylphosphatidylinositol (GPI)-phospholipase D overexpression on GPI metabolism. Biochem J *378*, 641-648.

Marin, R., Fabelo, N., Fernandez-Echevarria, C., Canerina-Amaro, A., Rodriguez-Barreto, D., Quinto-Alemany, D., Mesa-Herrera, F., and Diaz, M. (2016). Lipid Raft Alterations in Aged-Associated Neuropathologies. Curr Alzheimer Res *13*, 973-984.

Martinez, G., Duran-Aniotz, C., Cabral-Miranda, F., Vivar, J.P., and Hetz, C. (2017). Endoplasmic reticulum proteostasis impairment in aging. Aging Cell *16*, 615-623.

McGraw, P., and Henry, S.A. (1989). Mutations in the Saccharomyces cerevisiae opi3 gene: effects on phospholipid methylation, growth and cross-pathway regulation of inositol synthesis. Genetics *122*, 317-330.

Mizuno, T., Masuda, Y., and Irie, K. (2015). The Saccharomyces cerevisiae AMPK, Snf1, Negatively Regulates the Hog1 MAPK Pathway in ER Stress Response. PLoS Genet *11*, e1005491.

Mracek, T., Drahota, Z., and Houstek, J. (2013). The function and the role of the mitochondrial glycerol-3-phosphate dehydrogenase in mammalian tissues. Biochim Biophys Acta *1827*, 401-410.

Nakatsuka, A., Matsuyama, M., Yamaguchi, S., Katayama, A., Eguchi, J., Murakami, K., Teshigawara, S., Ogawa, D., Wada, N., Yasunaka, T.*, et al.* (2016). Insufficiency of phosphatidylethanolamine N-methyltransferase is risk for lean non-alcoholic steatohepatitis. Sci Rep *6*, 21721.

Ohno-Iwashita, Y., Shimada, Y., Hayashi, M., and Inomata, M. (2010). Plasma membrane microdomains in aging and disease. Geriatr Gerontol Int *10 Suppl 1*, S41-52.

Orlean, P. (2012). Architecture and biosynthesis of the Saccharomyces cerevisiae cell wall. Genetics *192*, 775-818.

Rep, M., Krantz, M., Thevelein, J.M., and Hohmann, S. (2000). The transcriptional response of Saccharomyces cerevisiae to osmotic shock. Hot1p and Msn2p/Msn4p are required for the induction of subsets of high osmolarity glycerol pathway-dependent genes. J Biol Chem *275*, 8290-8300.

Roberts, W.L., Myher, J.J., Kuksis, A., Low, M.G., and Rosenberry, T.L. (1988). Lipid analysis of the glycoinositol phospholipid membrane anchor of human erythrocyte acetylcholinesterase. Palmitoylation of inositol results in resistance to phosphatidylinositol-specific phospholipase C. J Biol Chem *263*, 18766-18775.

Romanauska, A., and Kohler, A. (2018). The Inner Nuclear Membrane Is a Metabolically Active Territory that Generates Nuclear Lipid Droplets. Cell *174*, 700-715 e718.

Sakakibara, K., Eiyama, A., Suzuki, S.W., Sakoh-Nakatogawa, M., Okumura, N., Tani, M., Hashimoto, A., Nagumo, S., Kondo-Okamoto, N., Kondo-Kakuta, C.*, et al.* (2015). Phospholipid methylation controls Atg32-mediated mitophagy and Atg8 recycling. EMBO J *34*, 2703-2719.

Sanjabi, B., Dashty, M., Ozcan, B., Akbarkhanzadeh, V., Rahimi, M., Vinciguerra, M., van Rooij, F., Al-Lahham, S., Sheedfar, F., van Kooten, T.G.*, et al.* (2015). Lipid droplets hypertrophy: a crucial determining factor in insulin regulation by adipocytes. Sci Rep *5*, 8816.

Sharma, N.K., Langberg, K.A., Mondal, A.K., and Das, S.K. (2013). Phospholipid biosynthesis genes and susceptibility to obesity: analysis of expression and polymorphisms. PLoS One *8*, e65303.

Shirra, M.K., Patton-Vogt, J., Ulrich, A., Liuta-Tehlivets, O., Kohlwein, S.D., Henry, S.A., and Arndt, K.M. (2001). Inhibition of acetyl coenzyme A carboxylase activity restores expression of

the INO1 gene in a snf1 mutant strain of Saccharomyces cerevisiae. Mol Cell Biol *21*, 5710-5722.

Singh, R.K., Fullerton, M.D., Vine, D., and Bakovic, M. (2012). Mechanism of hypertriglyceridemia in CTP:phosphoethanolamine cytidylyltransferase-deficient mice. J Lipid Res *53*, 1811-1822.

Sprenkle, N.T., Sims, S.G., Sanchez, C.L., and Meares, G.P. (2017). Endoplasmic reticulum stress and inflammation in the central nervous system. Mol Neurodegener *12*, 42.

Stein, A.J., and Geiger, J.H. (2002). The crystal structure and mechanism of 1-L-myo-inositol- 1-phosphate synthase. J Biol Chem *277*, 9484-9491.

Sukhai, M.A., Prabha, S., Hurren, R., Rutledge, A.C., Lee, A.Y., Sriskanthadevan, S., Sun, H., Wang, X., Skrtic, M., Seneviratne, A., *et al.* (2013). Lysosomal disruption preferentially targets acute myeloid leukemia cells and progenitors. J Clin Invest *123*, 315-328.

Summers, E.F., Letts, V.A., McGraw, P., and Henry, S.A. (1988). Saccharomyces cerevisiae cho2 mutants are deficient in phospholipid methylation and cross-pathway regulation of inositol synthesis. Genetics *120*, 909-922.

Tanaka, S., Maeda, Y., Tashima, Y., and Kinoshita, T. (2004). Inositol deacylation of glycosylphosphatidylinositol-anchored proteins is mediated by mammalian PGAP1 and yeast Bst1p. J Biol Chem *279*, 14256-14263.

Tao, Q., Ang, T.F.A., DeCarli, C., Auerbach, S.H., Devine, S., Stein, T.D., Zhang, X., Massaro, J., Au, R., and Qiu, W.Q. (2018). Association of Chronic Low-grade Inflammation With Risk of Alzheimer Disease in ApoE4 Carriers. JAMA Netw Open *1*, e183597.

Tardiff, D.F., Khurana, V., Chung, C.Y., and Lindquist, S. (2014). From yeast to patient neurons and back again: powerful new discovery platform. Mov Disord *29*, 1231-1240.

Taron, C.H., Wiedman, J.M., Grimme, S.J., and Orlean, P. (2000). Glycosylphosphatidylinositol biosynthesis defects in Gpi11p- and Gpi13p-deficient yeast suggest a branched pathway and implicate gpi13p in phosphoethanolamine transfer to the third mannose. Mol Biol Cell *11*, 1611-1630.

Thibault, G., Shui, G., Kim, W., McAlister, G.C., Ismail, N., Gygi, S.P., Wenk, M.R., and Ng, D.T. (2012). The membrane stress response buffers lethal effects of lipid disequilibrium by reprogramming the protein homeostasis network. Mol Cell *48*, 16-27.

Toh-e, A., and Oguchi, T. (2001). Defects in glycosylphosphatidylinositol (GPI) anchor synthesis activate Hog1 kinase and confer copper-resistance in Saccharomyces cerevisisae. Genes Genet Syst *76*, 393-410.

Toh-e, A., and Oguchi, T. (2002). Genetic characterization of genes encoding enzymes catalyzing addition of phospho-ethanolamine to the glycosylphosphatidylinositol anchor in Saccharomyces cerevisiae. Genes Genet Syst *77*, 309-322.

Toutant, J.P., Roberts, W.L., Murray, N.R., and Rosenberry, T.L. (1989). Conversion of human erythrocyte acetylcholinesterase from an amphiphilic to a hydrophilic form by phosphatidylinositol-specific phospholipase C and serum phospholipase D. Eur J Biochem *180*, 503-508.

Travers, K.J., Patil, C.K., Wodicka, L., Lockhart, D.J., Weissman, J.S., and Walter, P. (2000). Functional and genomic analyses reveal an essential coordination between the unfolded protein response and ER-associated degradation. Cell *101*, 249-258.

Treitel, M.A., Kuchin, S., and Carlson, M. (1998). Snf1 protein kinase regulates phosphorylation of the Mig1 repressor in Saccharomyces cerevisiae. Mol Cell Biol *18*, 6273-6280.

Vevea, J.D., Garcia, E.J., Chan, R.B., Zhou, B., Schultz, M., Di Paolo, G., McCaffery, J.M., and Pon, L.A. (2015). Role for Lipid Droplet Biogenesis and Microlipophagy in Adaptation to Lipid Imbalance in Yeast. Dev Cell *35*, 584-599.

von Toerne, C., Huth, C., de Las Heras Gala, T., Kronenberg, F., Herder, C., Koenig, W., Meisinger, C., Rathmann, W., Waldenberger, M., Roden, M.*, et al.* (2016). MASP1, THBS1, GPLD1 and ApoA-IV are novel biomarkers associated with prediabetes: the KORA F4 study. Diabetologia *59*, 1882-1892.

Wilson-Zbinden, C., dos Santos, A.X., Stoffel-Studer, I., van der Vaart, A., Hofmann, K., Reggiori, F., Riezman, H., Kraft, C., and Peter, M. (2015). Autophagy competes for a common phosphatidylethanolamine pool with major cellular PE-consuming pathways in Saccharomyces cerevisiae. Genetics *199*, 475-485.

Zheng, Z., and Zou, J. (2001). The initial step of the glycerolipid pathway: identification of glycerol 3-phosphate/dihydroxyacetone phosphate dual substrate acyltransferases in Saccharomyces cerevisiae. J Biol Chem *276*, 41710-41716.